Computational and Structural Biotechnology Journal 20 (2022) 5162–5180

COMPUTATIONAL ANDSTRUCTURAL BIOTECHNOLOGY JOURNAL

journal homepage: www.elsevier.com/locate/csbj

Structural communication between the GTPase Sec4p and its activator Sec2p: Determinants of GEF activity and early deformations to nucleotide release

Angelo Felline [a,1], Francesco Raimondi [a,c,1], Sara Gentile [a], Francesca Fanelli [a,b,*]

[a] Department of Life Sciences, University of Modena and Reggio Emilia, via Campy 103, 41125 Modena, Italy
[b] Center for Neuroscience and Neurotechnology, University of Modena and Reggio Emilia, via Campi 287, 41125 Modena, Italy
[c] Scuola Normale Superiore Pisa, Piazza dei Cavalieri, 7 – 56126 Pisa, Italy

ARTICLE INFO

Article history:
Received 19 July 2022
Received in revised form 8 September 2022
Accepted 8 September 2022
Available online 13 September 2022

Keywords:
Molecular dynamics simulations
Protein–protein docking
Ras GTPases
Guanine nucleotide exchange factor
Protein structure network
Structural communication

ABSTRACT

Ras GTPases are molecular switches that cycle between OFF and ON states depending on the bound nucleotide (i.e. GDP-bound and GTP-bound, respectively).

The Rab GTPase, Sec4p, plays regulatory roles in multiple steps of intracellular vesicle trafficking. Nucleotide release is catalyzed by the Guanine Nucleotide Exchange Factor (GEF) Sec2p.

Here, the integration of structural information with molecular dynamics (MD) simulations addressed a number of questions concerning the intrinsic and stimulated dynamics of Sec2p and Sec4p as well as the chain of structural deformations leading to GEF-assisted activation of the Rab GTPase.

Sec2p holds an intrinsic ability to adopt the conformation found in the crystallographic complexes with Sec4p, thus suggesting that the latter selects and shifts the conformational equilibrium towards a pre-existing bound-like conformation of Sec2p.

The anchoring of Sec4p to a suitable conformation of Sec2p favors the Sec2p-assisted pulling on itself of the α1/switch 1 (SWI) loop and of SWI, which loose any contact with GDP. Those deformations of Sec4p would occur earlier. Formation of the final Sec2p-Sec4p hydrophobic interface, accomplishes later. Disruption of the nucleotide cage would cause firstly loss of interactions with the guanine ring and secondly loss of interactions with the phosphates.

The ease in sampling the energy landscape and adopting a bound-like conformation likely favors the catalyzing ability of GEFs for Ras GTPases.

1. Introduction

Ras GTPases or G proteins (Guanine Nucleotide-Binding Proteins (GNBP)) are molecular switches that cycle between OFF and ON states depending on the bound nucleotide (i.e. GDP-bound (S^{GDP}) and GTP-bound (S^{GTP})) [1–3]. In the S^{GTP} active state, the G proteins display high affinity for binding downstream effectors, thereby controlling a variety of biological processes such as cell signaling, cell shape, motility and polarity, membrane transport pathways, transcription factor activity as well as vesicular or non-vesicular transport [1–3]. Differently from the small Ras GTPases, heterotrimeric G proteins of the Gα family hold a helical (H) domain in addition to the common GTPase (G) or Ras-like domain. As a Rab (Ras-related in brain) GTPase, Sec4p (hereafter indicated as Sec4) plays regulatory roles in multiple steps of intracellular vesicle trafficking [2]. One Rab can modulate and control an entire stage of transport including vesicle budding, delivery, docking, and fusion [4].

The switch-ON process is under the control of Guanine Nucleotide Exchange Factors (GEFs), which catalyze the exchange of GDP for GTP.

Each G protein family holds its own GEF. The cognate GEF of Sec4 is Sec2p (hereafter indicated as Sec2). GEF action involves a series of fast reaction steps, which lead from a binary GNPB-GDP complex via a trimeric GNBP-GDP-GEF complex to a binary nucleotide-free GNPB-GEF complex, which is stable in the absence of the nucleotide [1,3,5]. This series of reactions is reversed by rebinding of nucleotide, predominantly GTP, because of its higher concentration in the cell [6–8]. In this respect, the GEF acts as a

* Corresponding author at: Department of Life Sciences, University of Modena and Reggio Emilia, via Campi 103, 41125 Modena.
E-mail address: fanelli@unimo.it (F. Fanelli).
[1] Equally contributing authors listed in alphabetic order.

https://doi.org/10.1016/j.csbj.2022.09.016
2001-0370/

catalyst to increase the rate at which the equilibrium is pulled from S^{GDP} to S^{GTP}. Although Mg^{2+} contributes to the tight binding of nucleotides, GEFs further enhance nucleotide release even in the absence of Mg^{2+} (reviewed in Ref. [1,3,5]). Structure determinations and molecular simulations provided insights into the mechanism of G protein activation. MD simulations on small GTPases from different families revealed a common semi-open conformation similar to the GEF-bound state and suggested a regulatory role of Mg^{2+} [9]. MD simulations on a number of binary and ternary complexes of H-Ras served to infer changes in coordination of Mg^{2+} along the path to G protein activation [10]. The mechanism of GDP release distinguishes small GTPases from heterotrimeric G proteins, which employ G protein Coupled Receptors (GPCRs) as specialized GEFs. According to structure determination [11,12] and molecular simulations [13,14], uniquely to Gα proteins, GDP release catalyzed by GPCRs is accompanied by displacement of the H domain from the G domain.

The switch-OFF process is regulated by GTPase activating proteins (GAPs), which enhance the relatively slow intrinsic GTPase activity of G proteins. A number of simulation studies investigated nucleotide-dependent conformational states and the reaction path of GTP hydrolysis in small GTPases [15–19].

Like all Ras GTPases, Sec4 holds an αβα three-layer sandwich architecture and a Rossmann fold (Figs. 1 and 2)). The helices α1 and α5 lie on one side of the parallel β-sheet, whereas α2, α3, and α4 lie on the opposite side. The nucleotide docks into a binding site contributed by the β1/α1, α1/β2 (αF/β2 in the Gα proteins), β3/α2, β5/α4, and β6/α5 loops (i.e. G boxes 1–5 (G1-G5) Fig. 2 A,B). Sequence conservation over the Ras superfamily resides just in the G boxes, also defined as ultra-conserved regions (Fig. 1). G2 and G3 are also defined as switches I and II (SWI and SWII, respectively) and the β2-β3 hairpin preceded and followed by the switches is named inter-switch. Notably, SWII includes also the α2-helix (Fig. 1). Computational experiments suggested that the β1/β4 interface divides the Ras-like domain into two dynamically distinct lobes: lobe 1 (the *N*-terminal half of the domain) that includes the β1-β3 strands, the P loop, and the two switches; and lobe 2 (the C-terminal half) that includes the β4-β6 strands and the α3-α5 helices [15,21].

The crystal structures of the S^{GDP} and S^{GTP} states of Sec4, respectively bound to Co^{2+} and Mg^{2+} (PDB: 1G16 and 1G17, Fig. 2A,B) [22], show clear differences in the switch regions. Indeed, the transition to the active states induces two-residue lengthening of the N- and C-terminations of β2 and β3, respectively, and a one-turn extension of α2/SWII (Fig. 2A,B). As a consequence, in S^{GTP} the two switches become interacting forming the interaction Site 1 ($I55^{SWI:7}$-$W74^{β3:6}$-$Y89^{SWII:15}$) and Site 2 ($T51^{SWI:3}$-$Q79^{SWII:5}$ and $I53^{SW1:5}$-$F82^{SWII:8}$) (Fig. 2B). In both S^{GDP} and S^{GTP} crystal structures the nucleotide is caged by the G-boxes: whereas G1, G2, and G3 interact with phosphates and Mg^{2+}, G4, and G5 interact with the guanine base. G1 (P-loop or Walker A motif GxxxxGKS/T), G2 (or SWII), and G3 (participating in SWII) hold conserved glycines and essentially employ the backbone NH-groups to bind phosphates. The aspartate of DxxG (i.e. $D^{G3:1}$) in G3 (also called the Walker B motif) makes a water-mediated contact with Mg^{2+}, which is critically required for tight nucleotide binding and GTP hydrolysis in Ras GTPases. Together with the P-loop that interacts with the β-phosphate, the most important contributions to tight binding result from the interactions of the guanine base with G4 and G5. In this respect, specificity for guanine is realized by the aspartate side chain in position G4:4, which usually forms bifurcated H-bonds with the NH-group at position 1 and the NH_2-substituent at *C*2 of the guanine ring (Fig. 2A,B). The guanine ring makes also σ-π orthogonal interactions with F45 in the loop between α1 and SWI (Fig. 2A,B), whereas the ribose O3′ is engaged in H-bond with the backbone carbonyl oxygen atom of P47 in the same loop.

Nucleotide exchange requires, respectively, loss and gain of such interactions when GDP exits and GTP enters with the aid of the GEF domain of Sec2. In spite of the rather fast rate of nucleotide dissociation from Sec4, Sec2 is still capable to high efficiently stimulate nucleotide release [23].

The *N*-terminal domain of Sec2 is a prototype for a structurally distinct family of Rab GEFs, which forms a single 220 Å-long parallel coiled-coil (PDB: 2E7S [24], Fig. 2C). Insights into the mechanism of GDP release come from the crystal structures of PO_4^{3-}-bound and APO Sec4 in complex with the GEF domain of Sec2 (PDB: 2EQB [25] and 2OCY [26], respectively, Fig. 2D,E). The 2EQB complex with the P-loop of Sec4 bound to the phosphate ion represents an intermediary state compared to the 2OCY GDP-depleted state of the G protein. Furthermore, the crystal structure of Sec2 in complex with the GDP-bound Sec4-S29V mutant, characterized by reduction of both intrinsic and stimulated nucleotide exchange (PDB: 4ZDW [27]), may represent an intermediary state preceding GDP release. Remarkably, the structure of such Sec4 mutant does not hold Mg^{2+} indicating that such cation may be not essential for tight nucleotide binding to Sec4. In the crystal structures of Sec4-Sec2 complexes, Sec4 residues (45–58 and 81–89) in and around SWI and SWII all participate in the hydrophobic interface with the GEF. Such interface is contributed by: $F49^{SWI:1}$, $T52^{SWI:4}$, $I53^{SWI:5}$, $I55^{SWI:7}$, $F57^{SWI:9}$, $W74^{β3:6}$, $F82^{SWII:3}$, $I85^{SWII:6}$, and $Y89^{SWII:10}$ of Sec4 and F109, T105, and V101 from what we label as chain A of Sec2 (corresponding to chain B in 2E7S, 2EQB, and 2OCY structures) as well as L104 and L108 from what we label as chain B of Sec2 (corresponding to chain A in 2E7S and 2OCY and to chain C in 2EQB, Fig. 2C,D). Long-range salt bridge interactions at the interface include $K22^{β1:3}$-$E102^{Sec2A}$/$D103^{Sec2A}$, $R81^{SWII:7}$-$D103^{Sec2B}$ and D43-$K121^{Sec2A}$ (Fig. 2C,D). Remarkably, compared to the S^{GDP} state, F45 looses the interaction with the guanine ring of GDP and interacts with both $K121^{Sec2A}$ and $Y124^{Sec2A}$ (Fig. 2A, D,E). Sec2 favors the establishment of the interactions between the two Sec4 switches leading to formation of the S^{GTP} Site 1, whereas the amino acids in S^{GTP} Site 2 participate in the interface with Sec2 (Fig. 2B,D,E). Along the same line, Sec2 also favors lengthening of β2, β3, and α2 in preparation of the S^{GTP} state (Fig. 2B,D,E).

Collectively, structure determinations provided invaluable pictures of the inactive S^{GDP}, active S^{GTP}, Sec2-bound S^{APO}, and a couple of Sec2-bound intermediary states of Sec4. However, significant insights into the nucleotide exchange process may derive from molecular dynamics (MD) simulations. By simulating the dynamics of isolated Sec2 and of Sec4 in: a) complex with GDP-Mg^{2+} (S^{GDP}), b) complex with GTP-Mg^{2+} (S^{GTP}), c) a modeled quaternary complex with Sec2 and GDP-Mg^{2+} ($S^{GDP'}$), and d) a binary complex with Sec2, the present study addresses a number of questions concerning the intrinsic and stimulated dynamics of Sec2 and Sec4 as well as the chain of structural deformations leading to GEF-assisted activation of the Rab GTPase.

2. Methods

2.1. MD simulations

2.1.1. The input systems

Sub-microsecond and microsecond MD simulations in explicit water were carried out by the GROMACS (v4.0.7 [28]) package on the following systems: a) the crystal structures of the S^{GDP} (PDB: 1G16, $Sec4^{1G16}$) and S^{GTP} (PDB: 1G17, $Sec4^{1G17}$) states of Sec4 [22] with nucleotide, Mg^{2+} ion (in S^{GDP} Co^{2+} was replaced by Mg^{2+}), and coordinating water molecules; b) the crystal structure of nucleotide-free Sec4 in complex with Sec2 (following the elimination of the phosphate ion mimicking the β-phosphate of GDP in

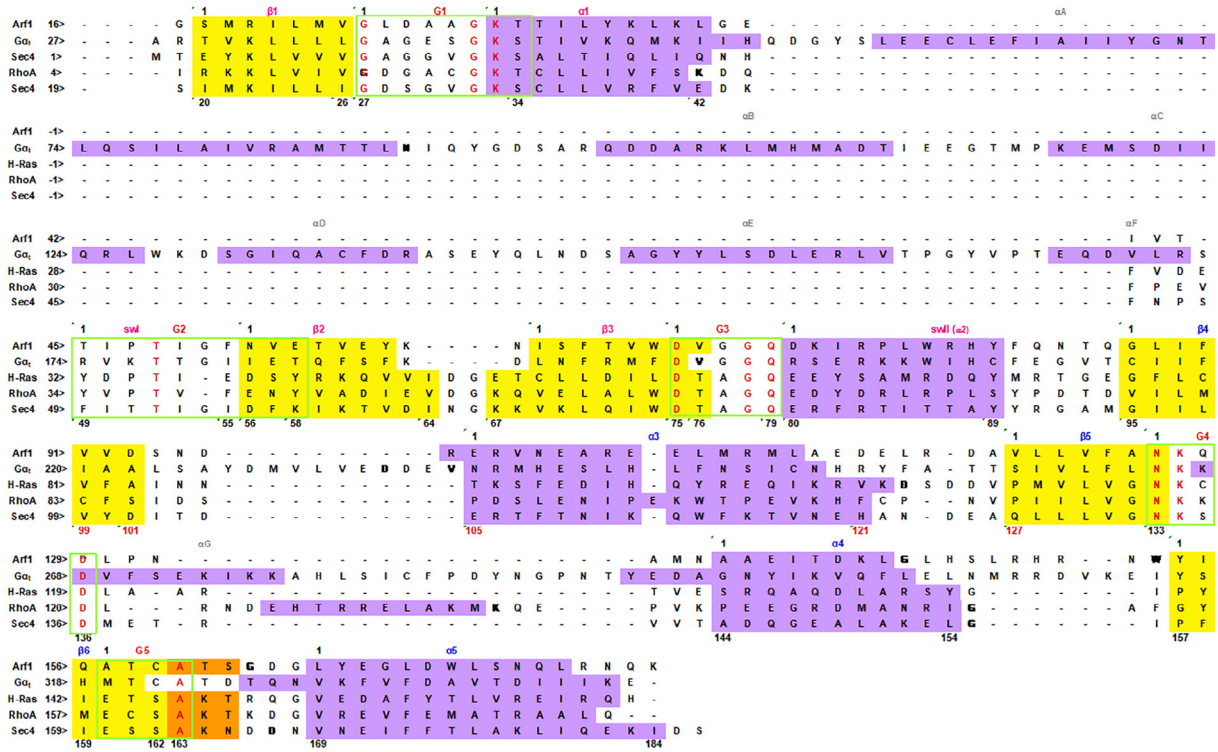

Fig. 1. Multiple sequence alignment of Arf1, Gα_t, H-Ras, RhoA, and Sec4. Canonical α-helices and β-strands are violet and yellow, respectively. The secondary structures herein reported, labeled according to the Noel's nomenclature, have been computed on the S^{GTP} state of the G proteins [20]. The G boxes are delimited by green boxes. Black numbers on the left side of the alignment refer to the sequential numbering, whereas black numbers above the sequences indicate the beginning of a secondary structure/G box motif. The fully conserved residues in such boxes are red. In order to facilitate *trans*-family comparisons, an arbitrary numbering was set characterized by the label of the secondary structure segment followed by the amino acid position in that segment. In those cases where the G-boxes overlap with the secondary structure segment, positions refer to the G-boxes. If G-boxes overlap with the switch regions, positional numbering refers to the latter portions. The amino acids in loops other than G-boxes hold the canonical sequential numbering. (For interpretation of the references to color in this figure legend, the reader is referred to the web version of this article.)

2EQB [25]) to probe the convergence towards the S^{APO} state; c) isolated Sec2 (PDB: 2E7S [24]); and d) Rosetta-predicted [29] complexes between GDP-bound Sec4 and Sec2 here defined as $S^{GDP'}$. In this respect, the crystallographic structures of $Sec4^{GDP}$ and unbound Sec2 (PDB: 1G16, chain C; 2E7S, chains A and B, residues 50–142, respectively), i.e. unbound-unbound docking, or $Sec4^{GDP}$ and Sec2 extracted from the complex with $Sec4^{APO}$ (PDB: 2OCY), i.e. unbound-bound docking, were used as inputs of protein–protein docking following the default RosettaDock protocol [29,30]. As for the unbound-unbound docking, the two proteins were pre-oriented by fitting each protein on the corresponding components of the Sec4-Sec2 complex (PDB: 2EQB, selected for the fitting because of the most complete structure of Sec4). As for the unbound-bound docking, only Sec4-GDP was pre-oriented upon fitting the structure onto Sec4 from the Sec2-Sec4 complex. In general, as for Sec2 fitting, either all or only the interfacial residues were considered, whereas, for Sec4 fitting, all residues except the two switch regions were considered. Before composing the input assemblies, the side-chain conformations of each docking partner were optimized by the "pre-packing" procedure [30]. For each input system, 1000 independent docking runs were done by randomly perturbing the initial orientation of the G protein [31]. For side-chain packing, extra-rotamers were used for all χ_1 dihedrals and for the χ_2 dihedrals of aromatic residues, including also rotamers from the unbound structures [31,32]. The best 200 poses, ranked according to the interface energy score [33], were retained from each docking assembly and evaluated for the number of interfacial native contacts, defined as those with at least one atom pair within 4 Å in the crystallographic complexes 2EQB or 2OCY. The top poses were subjected to interfacial residue-based clustering by means of Wordom [34], using a Cα-atom RMSD cutoff of 3 Å. Visual inspection of the top-scoring, most representative complex structures was instrumental in selecting 52 input complexes for MD simulations.

2.1.2. Simulation setup

Simulations were carried out by the GROMACS 4 (4.0.7) simulation package [28]. The AMBER03 all-atom force field was employed [35], using the TIP3P water model to explicitly describe the solvent. Available topologies and parameters for GDP and GTP for the AMBER force field were used [36]. Depending on the dimension of the system, a variable number of Na^+ and Cl^- ions were introduced to neutralize the system. Each simulation system was subjected to Periodic Boundary Conditions (PBC) with different unit cell boxes. In this respect, for isolated GTPases, an octahedric box with a distance of 12 Å between solute and boundaries was chosen, whereas for both the crystallographic and predicted Sec4-Sec2 complexes, 10 5 3 (xyz) box was used and aligned to the complex main axis. Such a box approximated the elongated shape of the Sec2 coiled-coil and reduced the number of solvating waters. To keep the principal axis of the complex aligned to the box main axis, translations and rotations of the mass center were removed during each simulation step.

All input structures were subjected to energy minimization using 500 steps of Steepest Descent, with an energy tolerance for convergence estimation of 1000 (kJ mol^{-1} nm^{-1}), followed by 500 steps of Conjugate Gradient, with an energy tolerance of 500 (kJ mol^{-1} nm^{-1}). The systems were then equilibrated for 4 ns of isothermal-isobaric (T = 300 K, P = 1 atm) MD simulations, restraining the position of all protein main-chain and Cβ atoms, nucleotide,

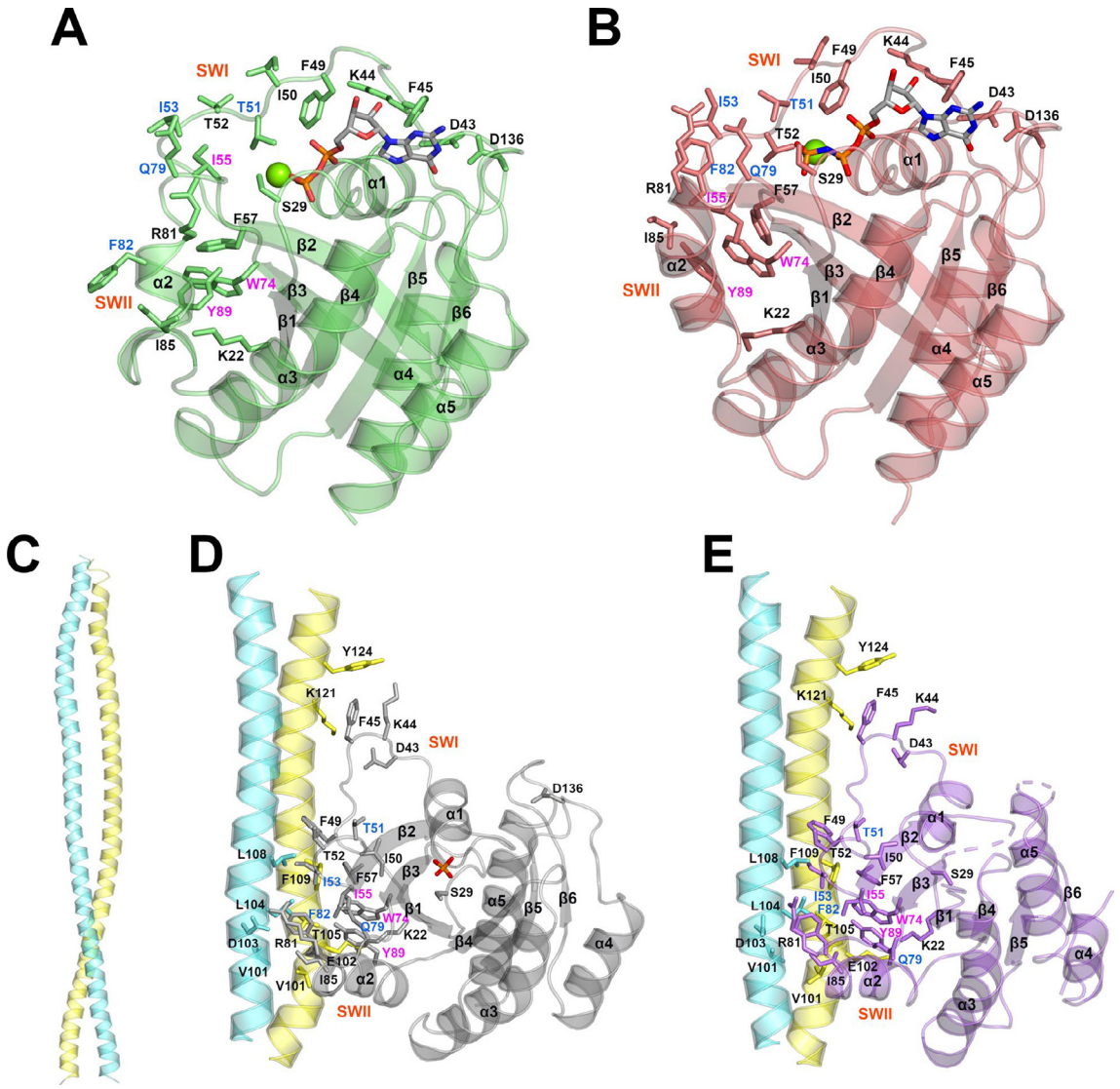

Fig. 2. Evidence from structure determinations. The crystal structures of Sec4 S^{GDP} (A, Protein Data Bank (PDB): 1G16), Sec4 S^{GTP} (B, PDB: 1G17), the dimeric GEF domain of Sec2 (C, PDB: 2E7S), the ternary complex between PO_4^{3-}-Sec4-Sec2 (D, PDB: 2EQB), and the binary complex Sec4-Sec2 (E, PDB: 2OCY) are shown. The labels of those amino acid residues, which in S^{GTP} participate in Site 1 and Site 2, are labeled magenta and blue, respectively. The two coiled-coil helices of Sec2 are yellow (labeled as chain A) and aquamarine (labeled as chain B), whereas the S^{GDP}, S^{GTP}, PO_4^{3-}-bound and APO Sec4 are, respectively, green, red, grey, and violet. The side chains participating in Sites 1 and 2 or in the interface between Sec4 and Sec2 are shown in sticks. Nucleotide and PO_4^{2-} ion are shown in sticks as well, colored by atom type. The Co^{2+} or Mg^{2+} ions in the 1G16 and 1G17 structures are represented as green spheres. The secondary structure elements are labeled according to the Noel's nomenclature [20]. (For interpretation of the references to color in this figure legend, the reader is referred to the web version of this article.)

Mg^{2+} and coordinating water molecules. The v-rescale thermostat [37] was employed to keep the system at a constant temperature of 300 K, using a coupling constant (τ^t) of 0.1 ps. The pressure of the system was kept fixed at 1 atm, using the Berendsen weak coupling algorithm [38] with a coupling constant (τ^p) of 1 ps. The Particle Mesh Ewald (PME) method was employed to compute electrostatic interactions, using a cutoff of 14 Å. Short-range repulsive and attractive interactions were computed using a Lennard-Jones potential with a cutoff of 12 Å. The LINCS algorithm [39] was used to allow for an integration time step of 2 fs by the leap-frog algorithm. The pre-equilibrated systems were then released for 1 ns prior to unrestrained MD simulations in the NPT ensemble (T = 300 K, P = 1 atm). For each crystallographic input structure, 5 independent replicas of 100 ns each were achieved by randomizing initial velocities.

For the $S^{GDP'}$ state, 52 Rosetta docking poses were subjected to 100 ns of unrestrained MD simulations (NPT ensemble). The trajectories showing some rearrangement towards the GEF-bound state were extended up to 1 μs. Herein only the analysis of the best conversion is shown. It is worth recalling that in the relative input complex, Sec4 is the crystallographic S^{GDP} state (PDB: 2G16), whereas Sec2 comes from the crystallographic complex with Sec4 APO (PDB: 2OCY). All simulations arising from unbound-unbound input complexes (i.e. with both Sec4 and Sec2 from their unbound inactive crystallographic structures, 1G16 and 2E7S, respectively) did not produce acceptable transitions.

The time series of Cα-Root Mean Square Deviations (Cα-RMSDs) concerning S^{GDP}, S^{GTP}, $S^{GDP'}$, and S^{APO} are shown in Supplementary Fig. 1 (Figure S1).

2.2. MD analyses

Comparative analyses of the MD trajectories of the different Sec4 and Sec2 states were carried out by the in-house software Wordom [34] and PSNtools [40].

Incidentally, to save clarity, we renamed as chain A what is called chain B in 2E7S, 2EQB, and 2OCY structures, whereas we renamed as chain B what is called chain A in 2E7S and 2OCY and chain C in 2EQB.

2.2.1. Analysis of flexibility

MD trajectories were subjected to a variety of analyses aimed at inferring the intrinsic flexibility of the systems (i.e. Cα-RMSDs, Cα-Root Mean Square Fluctuations (Cα-RMSFs), force constants [41–43], overall fluctuations [44], collective motions by Principal Component Analysis (PCA) [45], as well as functional mode Analysis (FMA) [46]. As for FMA, it consists in searching for possible correlations between structural features and essential motions, by using the Pearson Coefficient. In this framework, several size/shape and intermolecular interaction descriptors were correlated with linear combinations of a variable number of PCs. All these analyses were performed by means of the Wordom software [34]. All structural descriptors were computed by Wordom as well [34].

For a selection of computational indices, a detailed description is shown as follows.

As for force constants, the mechanical properties at the single residue level were inferred by computing the residue force constants through the analysis of the mean fluctuation of the mean distance d_i from each residue (to the rest of the structure) along the MD trajectory according to the following formula:

$$k_i = \frac{3k_BT}{\langle (d_i - \langle d_i \rangle)^2 \rangle} \quad (1)$$

where d_i is the mean distance defined above, <> denotes the average over the simulation, k_B is the Boltzmann constant, and T is the simulation temperature.

Protein dynamics was also investigated by computation of the overall fluctuation index Θ, which is a measure of the intrinsic flexibility of the whole protein (or of a given sub-set of residues) and is proportional to the extent of conformational space explored in a simulation [44]. Θ is defined as root mean distance variance of each atom pair and is calculated by the following equation:

$$\Theta_{AB} = \sqrt{\frac{\sum_{i=1}^{N}\sum_{j=1}^{M}\frac{\sum_{k=1}^{F}\left(d_{ij}^{k}-\overline{d_{ij}}\right)^2}{F}}{N \times M}} \quad (2)$$

where *A* and *B* are two sets of residues, *N* and *M* are the total number of atoms in set *A* and set *B*, respectively, and *F* is the total number of trajectory frames. Furthermore, d_{ij}^{k} is the distance between atom *i* from residue set A and atom *j* from residue set B in the k^{th} frame while $\overline{d_{ij}}$ is the average distance between the same two atoms. Here we considered all Cα-atoms in each helix, strand, G box, switches, and the C1 atom of the nucleotide to define the sets of amino acid residues for mean pairwise distance variance computation.

Comparisons of the overall fluctuations of such residue sets between S^{GDP} and S^{GTP}, between S^{APO} and S^{GDP} or $S^{GDP'}$, and between S^{GDP} and $S^{GDP'}$ were computed according to the following formulas:

$$\Delta\Theta\% = 100 - \frac{\Theta min}{\Theta max} * 100 \quad (3)$$

where Θ*min* and Θ*max* indicate, respectively, the states with minimal and maximal Θ values.

As for PCA of the different Sec4 or Sec4-Sec2 states, the covariance matrices were built on the Cα-atoms of the isolated MD trajectories by fitting all Cα-atoms. The same fitting strategy was employed to compute the Cα-RMSF.

2.2.2. Analysis of the structural communication by the protein structure networks

The structural communication was investigated by the protein structure network (PSN) analysis implemented in the PSNtools [40]. PSN analysis is a product of graph theory applied to protein structures [47]. The methodological approach for computing the structure graph and the shortest communication pathways has been described in a number of research articles [40,48,49].

Shortly, in a PSN, each linked residue (e.g. amino acid, nucleotide, small molecules, ion, etc) is a node [50]. Links form if the non-covalent interaction strength between pairs of nodes equals or overcomes a cutoff (I_{min}). Such interaction strength, expressed as a percentage, is computed by the equation (4) below:

$$I_{ij} = \frac{nij}{\sqrt{N_i N_j}} \times 100 \quad (4)$$

where I_{ij} is the percentage interaction between residues i and j; n_{ij} is the number of heavy atom–atom pairs between the side chains of residues i and j within a distance cutoff (4.5 Å); N_i and N_j are normalization factors for residue types i and j, which account for their propensities to make contacts with surrounding residues [47,51]. As for the normalization factors, the PSNtools software employs an internal database holding the normalization factors for the 20 standard amino acids and the 8 standard nucleotides (i.e. dA, dG, dC, dT, A, G, C, and U), as well as for more than 35,000 molecules (e.g. small molecules, lipids, sugars, etc) and ions extracted from all the structures deposited to date in the PDB. The normalization factors for GDP, GTP, and Mg^{2+} employed in this investigation are 246.47, 248.84, and 19.76, respectively.

Thus, the interaction strengths (I_{ij}) are computed for all node pairs. At a given interaction strength cutoff, I_{min}, any residue pair ij for which $I_{ij} \geq I_{min}$ (see equation Eqn 4) is considered to be interacting and hence is connected. The I_{min} cutoff is automatically computed as described in a recent paper [40]. In more detail, the I_{min} employed for the PSN analysis on MD simulations is the average over all the I_{min} computed on each trajectory frame.

Only those links and hubs present in at least 33% of the trajectory frames were defined as stable and considered for further analysis.

To avoid excessive network fragmentation, which would impair the search for shortest communication pathway, all node clusters (i.e. ensembles of nodes connected by at least one link) were iteratively connected by the link with the highest sub-cutoff interaction strength.

The allosteric communication was studied by searching for the shortest communication pathways. A pathway describes how signals are transferred between sites and consists of a set of residues in dynamic contact [52,53]. The procedure for computing the shortest communication pathways, which has been previously described and validated [40,49], is based on Dijkstra's algorithm [54].

A coarse/global picture of the whole structural communication in the considered system is provided by consensus paths or metapaths made of the most recurrent links in the path pool (i.e. with a recurrence ≥ 20% in this study) [40].

2.3. Analysis of amino acid conservation

Conservation analysis was performed by using the ConSurf web server (https://consurf.tau.ac.il) [55]. In a typical ConSurf applica-

tion, the query protein is first BLASTed against the UNIREF-90 database. Redundant homologous sequences are then removed using the CD-HIT clustering method. The resulting sequences are next aligned and the generated multiple sequence alignment (MSA) is used to reconstruct a phylogenetic tree. Given the tree and the MSA, the Rate4Site algorithm is used to calculate position-specific evolutionary rates under an empirical Bayesian methodology. The rates are normalized and grouped into nine conservation grades 1-through-9, where 1 includes the most rapidly evolving positions, 5 includes positions of intermediate rates, and 9 includes the most evolutionarily conserved positions [55]. We employed the sequences in the crystal structures of Sec4 (PDB: 1G16) and Sec2 (PDB: 2EQB) to run the ConSurf analysis.

3. Results

3.1. Functional dynamics of Sec2, Sec4, and their mutual association

The main goals of the present investigation are to explore the intrinsic dynamics of: a) the Sec2 GEF homodimer, b) Sec4 in ternary complex with hydrated Mg^{2+} and either GDP (S^{GDP}) or GTP (S^{GTP}), c) APO-Sec4 in complex with Sec2 starting from the PO_4^{3-}-bound intermediary state of the Rab protein (S^{APO}), and d) the Sec2-induced transition of Sec4 from S^{GDP} to S^{APO}. The goals were accomplished by comparative MD simulations followed by several structural analyses by established approaches already employed to investigate dynamics and structural communication in a number of Ras GTPases [14,56–61].

3.1.1. The intrinsic dynamics of Sec2 suggests conformation selection by Sec4

Since the minimal Sec2 sequence required for formation of a stable complex with Sec4 and to exert a GEF action is the region 51–142 [27], all simulations considered only the 50–142 Sec2 segment.

Clear structural differences emerge from comparisons of the free (i.e. 2E7S [24]) and Sec2-bound states (i.e. the crystal structures 2EQB, 2OCY, and 4ZDW) of Sec2. The relative orientation of the two helices around the Sec4 binding site (100–121 region) is conserved in all the 10 $Sec2^{31\text{-}160}$ dimers in the crystallographic asymmetric unit of $Sec2^{31\text{-}160}$ (i.e. 2E7S). Such orientation changes in the complex with Sec4. Indeed, in free Sec2 the two helices cross by 20° in the 100–121 region (inter-main-axis angle = 21.67° for chains A and B of 2E7S, Fig. 3A), whereas in the complexes with Sec4 the two helices are almost parallel (inter-main-axis angle = 7.54° for 2OCY (Fig. 3A) and 9.43° for 2EQB). Other remarkable structural changes between free and Sec4-bound Sec2 concern the patterns of inter-helix interactions in the 100–80 region, which reflects on changes in inter-helical distances.

In detail, in free Sec2 (i.e. $Sec2^{2E7S}$) the two R87 side chains hold almost extended conformations and point towards the main axis of the opposite helix, $R87^{Sec2A}$ making H-bond with $N84^{Sec2B}$ and $R87^{Sec2B}$ making a salt bridge with $E91^{Sec2B}$ (Fig. 3A).

Remarkably, in the crystallographic complexes with Sec4 (e.g. $Sec2^{2OCY}$), the two arginines make salt bridges respectively with D83 on the opposite helix, favoring the approaching of the helix main axes (Fig. 3A). Furthermore, in free Sec2, $A94^{Sec2A}$ and $A90^{Sec2B}$ are distant, being instead interacting in the bound state. Moreover, $F94^{Sec2A}$ makes contacts with both $L104^{Sec2B}$ and $L108^{Sec2B}$, contributing to the coiled-coil interface (Fig. 3A).

Very interestingly, MD simulations of free Sec2, starting from the 2E7S structure (chains A and B), show that the majority of frames hold the two helices almost parallel around the Sec4 binding site (region 100–121, Fig. 3A,B), the median angle between the helix main axes being 7.04 ± 4.24° (Fig. 3B). Along this line, the coiled-coil interface tends to approximate the one of crystallographic Sec4-bound Sec2, the frame closest to $Sec2^{2OCY}$, $Sec2^{MD}$, holding a Cα-atom RMSD 1.82 Å from $Sec2^{2E7S}$ input structure and equal to 0.90 Å from $Sec2^{2OCY}$ (see the left and right insets of Fig. 3B). Remarkably, side-chain interactions at the coiled-coil interface overlap as well between $Sec2^{MD}$ and $Sec2^{2OCY}$ (Fig. 3A). Along the same line, the pattern of inter-helical distances along the 50–142 sequence diverges for $Sec2^{2E7S}$ and $Sec2^{2OCY}$ crystal structures, whereas it overlaps extraordinary well for $Sec2^{MD}$ and $Sec2^{2OCY}$ (Fig. 3C).

Consistently, the distributions of the first five PCA projections clearly show that isolated Sec2 (i.e. $Sec2^{MD}$, Figure S2) explores a wider essential sub-space than Sec2 bound to Sec4 (i.e. $Sec2^{APO}$, Figure S2). In all pairwise combinations of PCs, a partial overlap occurs between the subspaces explored by $Sec2^{MD}$ and $Sec2^{APO}$ (Figure S2).

Collectively, these results unequivocally indicate that free Sec2 is able to adopt a Sec4-bound state even in the absence of Sec4, thus suggesting that the G protein likely selects a pre-formed Sec2 conformation prone to form a productive complex.

3.1.2. Nucleotide and Sec2-GEF affect the intrinsic flexibility of Sec4

The crystal structures of Sec4 provided significant insights into the structural features of the functionally different states of the G protein. The transition from the inactive S^{GDP} ($Sec4^{1G16}$ structure, Fig. 2A) to the active S^{GTP} ($Sec4^{1G17}$ structure, Fig. 2B) involves folding of SWII in a longer α-helix and a re-organization of the interface between the two switches with formation of two interaction sites in S^{GTP} (Fig. 2A,B). Such process passes through the interaction of both switches with Sec2, which leads to the GEF-bound S^{APO} state of the G-protein ($Sec4^{2OCY}$ structure, Fig. 2E). Early stages in nucleotide release are represented by the crystal structures of Sec4 bound to both Sec2 and GDP ($Sec4^{4ZDW}$) or to Sec2 and PO_4^{3-} ($Sec4^{2EQB}$, Fig. 2D).

To investigate the intrinsic dynamics of S^{GDP}, S^{GTP}, and S^{APO} states the crystal structures $Sec4^{1G16}$, $Sec4^{1G17}$, and $Sec4^{2EQB}$ deprived of PO_4^{3-} were used as inputs of MD simulations. Exploration of the conformational ensembles associated to the three Sec4 states was complemented by simulation of a S^{GDP} transition to a Sec2-bound form (i.e. $S^{GDP'}$) by using a modeled complex between $Sec4^{1G16}$ and $Sec2^{2OCY}$ as an input (see the Experimental Section).

Cα-RMSFs remark evidence from computational experiments that in S^{GDP} and S^{GTP} of Ras GTPases flexibility essentially concerns the SWI ($49\text{-}55^{Sec4}$) and SWII ($75\text{-}89^{Sec4}$) regions, which are more flexible in S^{GDP} than S^{GTP} (Fig. 4) [56,59,61]. In the predicted $S^{GDP'}$, the flexibility of SWII is the highest compared to the other states. Unique feature to S^{APO} is the higher flexibility of the α1/β1-loop or P-loop (G1), α1, α3, G4, and G5 compared to all other forms (Fig. 4), whereas SWI shows the lowest flexibility likely due to the intermolecular interactions with Sec2. In general, helices show higher flexibility than β-strands due to the αβα-sandwich architecture that buries the β-sheet by the two layers of α-helices. The higher flexibility of the G-boxes G1, G4, and G5 in S^{APO} is likely due to the lack of the nucleotide and is in line with the observations that loops in the Sec4 nucleotide-binding pocket are disordered as a consequence of nucleotide removal [26].

The mechanical properties of the considered systems at a single-residue level were computed by inferring the force constant from the mean fluctuations of the mean distance from each residue with respect to the rest of the protein structure (see the Experimental Section) [41–43]. Force constants are almost complementary to Cα-RMSFs, in the sense that major rigidity (i.e. increase in force constants) concerns regions with lower flexibility (Fig. 5A-D). In this respect, the most rigid regions are, as expected, the β-strands participating in the parallel β-sheet with more prominence

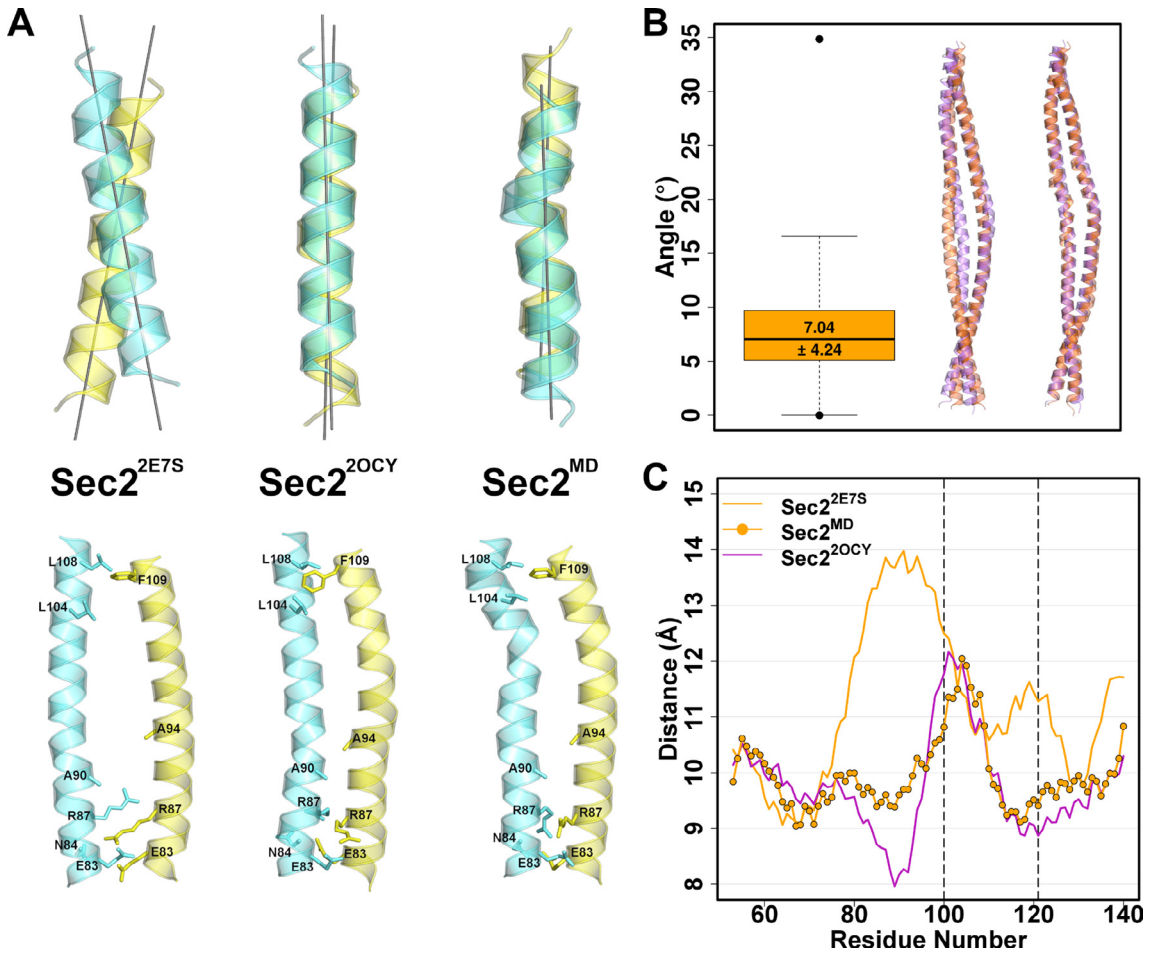

Fig. 3. Intrinsic dynamics of Sec2. A, top. The helix main-axis orientations of the 100–121 region of Sec2 crystallized in its isolated state ($Sec2^{2E7S}$), in complex with Sec4 ($Sec2^{2OCY}$), or simulated in the isolated state ($Sec2^{MD}$) are shown. Helices A and B are shown as yellow and aquamarine cartoons, respectively. As for $Sec2^{MD}$, the frame closest in Cα-RMSD to $Sec2^{2OCY}$ is shown. A, bottom. A different view of sections 81–110 of the two helices is shown for $Sec2^{2E7S}$, $Sec2^{2OCY}$, and $Sec2^{MD}$. B. The superimposed structures of $Sec2^{2OCY}$ (violet) with $Sec2^{2E7S}$ (left orange) and with $Sec2^{MD}$ (right orange) are shown. The orange boxplot reports the median value and the standard deviation of the angle between the helix-main exes in the region 100–121. The two black lines extending from the box indicate the variability outside the upper and lower quartiles and the two black dots represent the largest and lowest values of the angle. C. The distances between the α-helix axes in $Sec2^{2E7S}$ (orange line), $Sec2^{2OCY}$ (violet line), and $Sec2^{MD}$ (orange line with circles) are plotted. The distance between the α-helix axes of Sec2, as a function of residue number, is calculated as the distance between the projections of the geometric backbone-atom center of each residue on the local helix main axis. For each residue, the local main axis of each helix is recalculated using the backbone coordinates of the residue and of the six preceding and following residues (in the primary sequence). (For interpretation of the references to color in this figure legend, the reader is referred to the web version of this article.)

to β1 and β4, which are adjacent in space and occupy inner positions in the β-sheet. This behavior is due to the three-layer αβα architecture of the Rossmann fold, independently of the functional state. Highly conserved amino acids (i.e. with ConSurf grades ≥ 7) tend to hold force constants above the average, consistent with the demonstrated relationships between amino acid mechanical rigidity, evolutionary conservation, and belonging to the folding nucleus in 70 protein structures from 14 protein families [62]. In this respect, the β4-strand, which marks the beginning of the C-terminal half of the G protein, shown to be dynamically distinct from the *N*-terminal one [59], reaches the highest rigidity level in all forms, S^{APO} showing a lower level of rigidity in its C-terminal half, excluding α5, than the other forms (Fig. 5). In this respect, we remark that $D136^{G4:4}$, a stable and mechanically rigid anchoring point for the nucleotide in all nucleotide-bound forms, acquires flexibility in S^{APO} (Fig. 5). Importantly, in S^{APO}, the mechanical rigidity of the P-loop goes below the average, being above the average in all nucleotide-bound forms.

As for the overall fluctuations, SWI and SWII tend to fluctuate in tandem with each strand, helix, and G box (Fig. 6). Major divergences concern S^{GDP} and S^{GTP} states, the former showing remarkably higher fluctuations than the latter (Fig. 6A). Indeed, pairwise comparisons between the different states show that, in S^{GDP}, SWI, SWII, inter-switch, and nucleotide display higher overall fluctuation than they do in S^{GTP} (Fig. 6A). In S^{GDP}, SWI and inter-switch fluctuate in tandem with the other Sec4 portions more than they do in the predicted complex between $Sec4^{1G16}$ and $Sec2^{2OCY}$ (i.e. $S^{GDP'}$) (Fig. 6B). Remarkably, $S^{GDP'}$ is closer in overall fluctuations to S^{APO} than to S^{GDP} (Fig. 6B-D), not only because both $S^{GDP'}$ and S^{APO} concern GEF-bound forms, but also because $S^{GDP'}$ likely represent an evolution of S^{GDP} towards the nucleotide-depleted form. In both the simulated GEF-bound forms, the whole Sec2 shows overall fluctuations with all Sec4 portions, which are higher in $S^{GDP'}$ than S^{APO}, suggesting that the former complex is more dynamic and less stable than the latter (Fig. 5D).

Collectively, despite the presence of bound GDP and Mg^{2+}, the flexibility of Sec4 in $S^{GDP'}$ resembles that of S^{APO} more than S^{GDP}, indicating that $S^{GDP'}$ expresses an evolution towards nucleotide release. The nucleotide-depleted S^{APO} form shows enhanced flexibility of the P-loop and the C-terminal half than the other forms, which may be linked to the structural rearrangements preventing GDP rebinding [25].

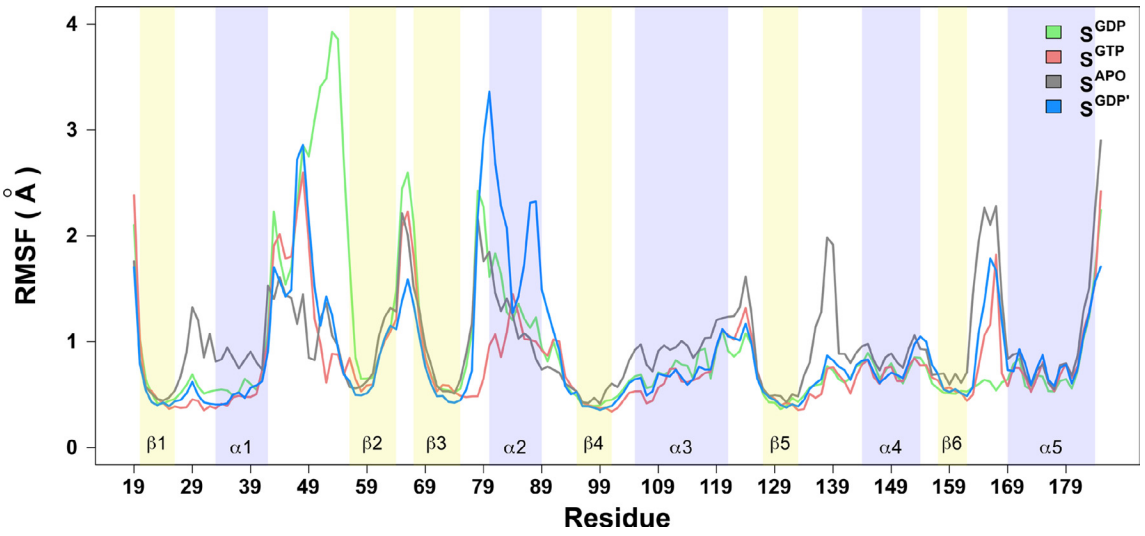

Fig. 4. Flexibility profiles of the different Sec4 forms. The Cα-RMSFs profiles from the MD trajectories of S^{GDP} (green), S^{GTP} (red), S^{APO} (grey), and $S^{GDP'}$ (marine) are shown. Background colors indicate the secondary structure of the amino acid residues, where violet, yellow, and white indicate, respectively, helices, strands, and loops. (For interpretation of the references to color in this figure legend, the reader is referred to the web version of this article.)

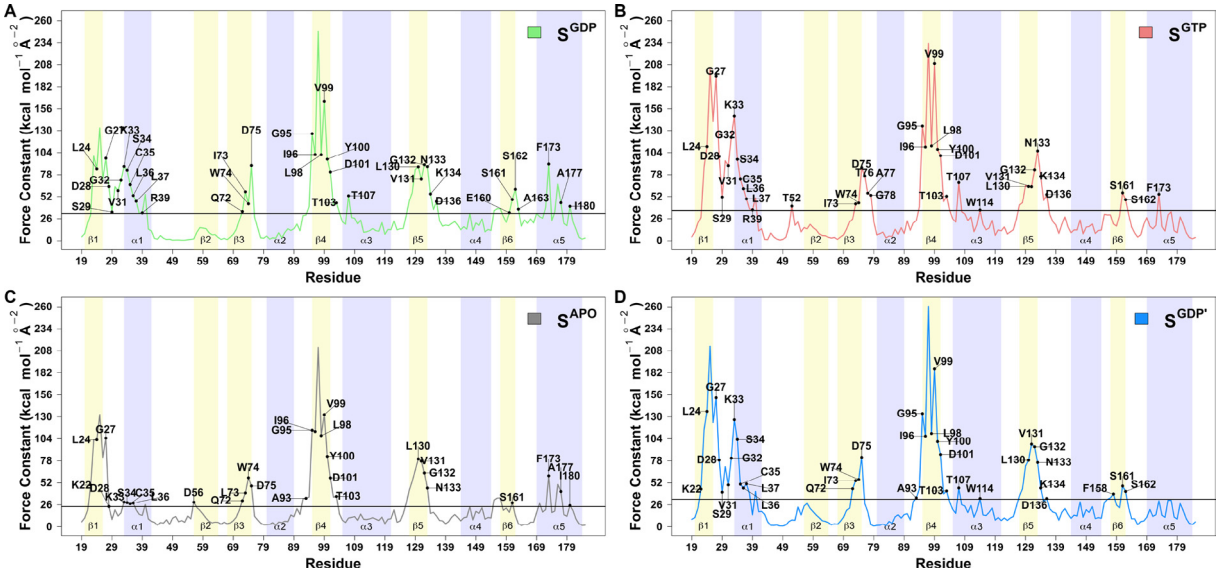

Fig. 5. Mechanical rigidity profiles of Sec4. The force constant profiles from the MD trajectories of S^{GDP} (green), S^{GTP} (red), S^{APO} (grey), and $S^{GDP'}$ (marine) are shown. The numbers on mechanical profiles highlight the amino acids holding both force constant ≥ the average (black line) and ConSurf conservation color ≥ 7. (For interpretation of the references to color in this figure legend, the reader is referred to the web version of this article.)

The analysis of Sec4 crystal structures allowed us to define a number of structural hallmarks of the different functional states. Such hallmarks, computed on the trajectory frames, contributed to infer hypotheses on the mechanism of nucleotide exchange.

In this respect, we tested a huge number of descriptors finally selecting the following: a) the distance between the Cα-atom of $G32^{G1:6}$ and the centroid of the $F49^{SWI:1}$ side chain; b) the angle among the Cα-atoms of $R39^{\alpha1:7}$, $S34^{G1:8}$, and K44; and d) the angle between the main axes of the α2 and α3 helices (by selecting, respectively, the amino acid ranges 86–91 and 113–118 for S^{GDP}, S^{GTP}, and $S^{GDP'}$ and 82–91 and 112–122 for S^{APO}) (Fig. 7).

Whereas the G32-F49 distance and the angle between the three Cα-atoms describe the deformations of P-loop (G1) and SWI (G2), the angle between α2 and α3 describes deformations of SWII (G3) associated with changes in G protein functional state. Indeed, all those descriptors increase ongoing from the S^{GDP} or S^{GTP} isolated states of Sec4 to its Sec2-bound forms. In particular, in Sec2-bound forms the main axes of α2 and α3 become almost orthogonal following rotation of α2, while participating in the interface with Sec2. The pairwise combinations of the three indices computed on the trajectory frames were effective in distinguishing the different states of Sec4 and highlight the tendency of the conformational ensembles to deviate from the input structure (Fig. 8A-D). In detail, independently of the index, the population-surfaces show the basins of the Sec2-bound forms of Sec4 ($S^{GDP'}$ and S^{APO}) clearly separated from the unbound ones and shifted towards higher values of all three indices (Fig. 8). S^{GDP} and S^{GTP} show more than one basin deviating from the position of the crystallographic input structure. This behavior that is emphasized in S^{GDP} compared to S^{GTP}, is due to the intrinsic flexibility the two switches. Remarkably, the most

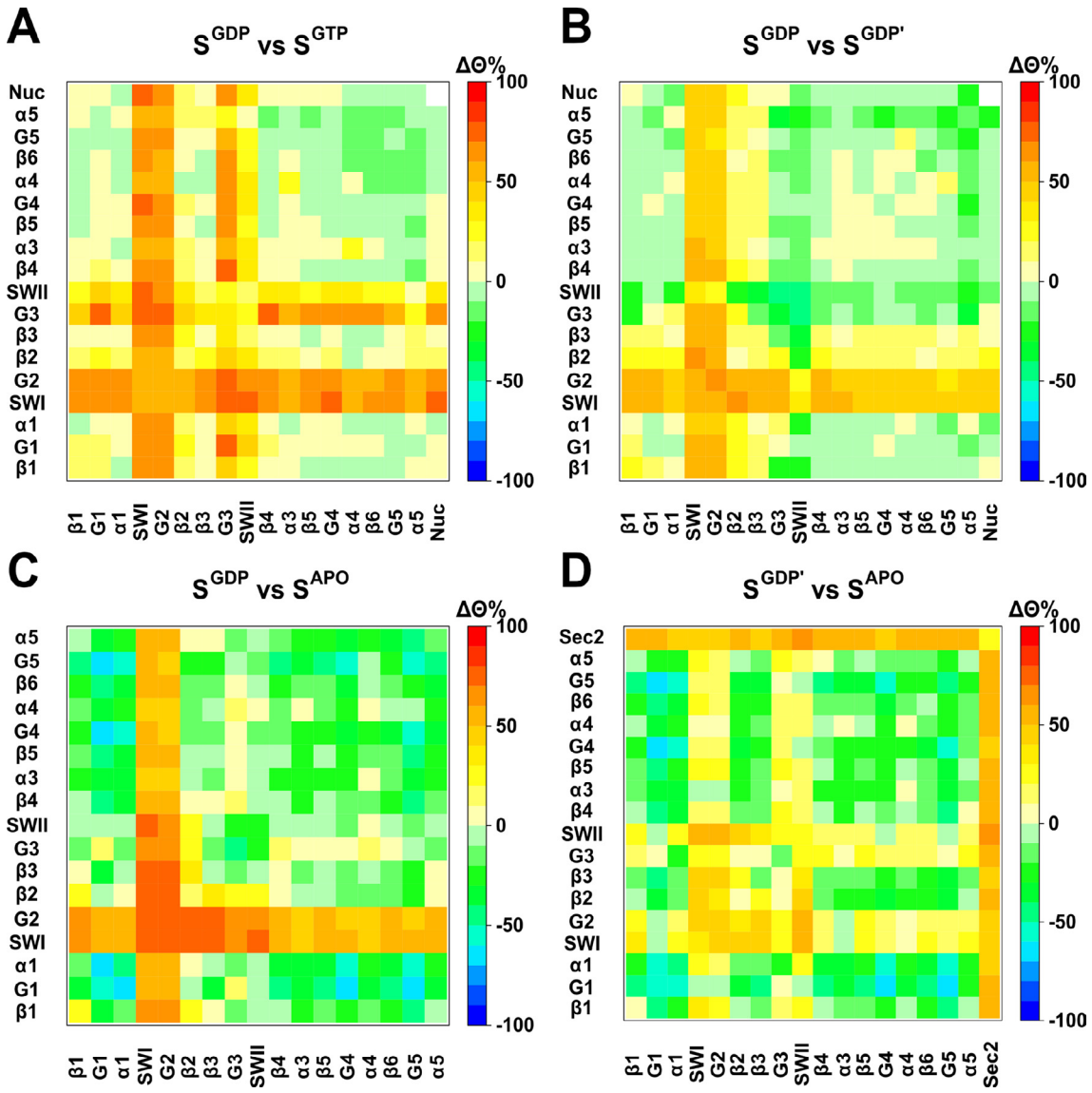

Fig. 6. Comparisons of the overall flexibility of the different Sec4 states. Pairwise % differences in overall fluctuations between the different portions are expressed as colors in the matrices (see the color legend on the right). The four panels show comparisons between: (A) S^{GDP} and S^{GTP}, (B) S^{GDP} and $S^{GDP'}$, (C) S^{GDP} and S^{APO}, and (D) $S^{GDP'}$ and S^{APO}. The sign of the Δ% is relative to the second state listed on each matrix.

relevant deviation from the input structure concerns $S^{GDP'}$ since the Sec4 input structure, i.e. the crystallographic structure $Sec4^{1G16}$ (Fig. 8A), during MD simulations evolves towards the crystallographic structures $Sec4^{2EQB}$ or $Sec4^{2OCY}$ (Fig. 8A) as well as towards the conformational ensemble of S^{APO} (Fig. 8B-D). The single basin of the S^{APO} conformational ensemble tends to remain close to the input structure (Fig. 8A-D).

The geometrical descriptors listed above worked well in functional mode analysis (FMA) computed on the different states of Sec4. Indeed, all of them correlated with the collective atomic motions describing the essential subspace (ES) of Sec4 in different functional states. In general, ES is contributed by a variable number of eigenvectors whose associated eigenvalues account for 90 % of the total variance of the Cα-displacements in a trajectory.

In this study for all considered states of Sec4, the R39-S34-K44 and α2/α3 angles gave correlations $R^2 \geq 0.93$ (validation set) and $R^2 \geq 0.97$ (model set) with a combination of the first 500 eigenvectors describing ~100% of the total variance of the Cα-displacements (i.e. the ES).

As for the α2/α3 angle, correlations concerning both validation and model sets were relatively low (R^2 = 0.70) only for S^{APO}. The G32-F49 distance performed slightly worse, since the correlation coefficients $R^2 \geq 0.85$ (validation set) or $R^2 \geq 0.97$ (model set) were achieved for all systems but S^{GDP}, which did not provide correlations above 0.7 R^2. For each system, the projections on the Cα-atoms of the weighted combination of the first 500 eigenvectors described the same collective motions. Weighing of eigenvectors was based on their contribution to the FMA correlative model. Therefore, here we show only the projections concerning the collective motions correlated with variations of the R39-S34-K44 angle as exemplar of the collective motions correlated with the other two descriptors (Fig. 9). In general, the weighted combination of the first 500 eigenvectors describes collective motions of SWI. Whereas for S^{GDP} and S^{GTP} such modes involve exclusively SWI (Fig. 9A,B), for $S^{GDP'}$ they involve an increasing number of portions, as SWI, SWII, inter-switch, G5, and α5 (Fig. 9C). Remarkably, largest amplitude motions concern SWI, which displaces towards the Sec2 GEF (Fig. 9C). For the S^{APO} collective motions, even if with

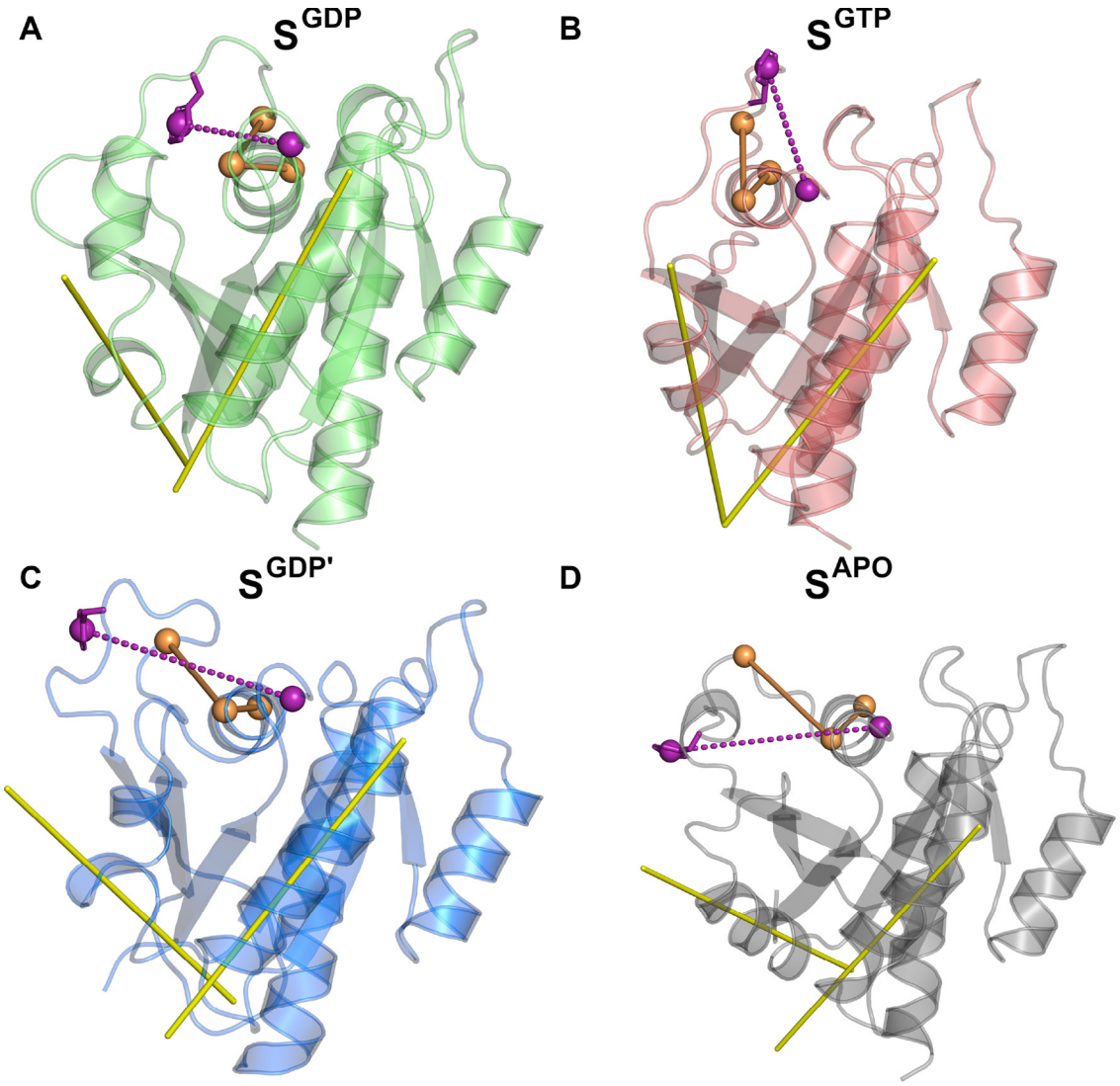

Fig. 7. Structural hallmarks of Sec4 states. The distance between the side-chain centroid of $G32^{G1:6}$ and $F49^{G2:1}$ (purple), the angle among the Cα-atoms of $R39^{a1:7}$, $S34^{G1:8}$, and K44 (orange), and the angle between the main axes of the α2 and α3 helices (yellow) are shown on the structures of (A) S^{GDP} (green), (B) S^{GTP} (red), (C) $S^{GDP'}$ (marine), and (D) S^{APO} (grey) closest in Cα-RMSD to the average structure from the relative MD trajectory. (For interpretation of the references to color in this figure legend, the reader is referred to the web version of this article.)

lower amplitude compared to $S^{GDP'}$, involve all Sec4 portions, likely linked to the presence of Sec2 and to removal of the PO_4^{3-} ion mimicking the nucleotide β-phosphate in the $Sec4^{2EQB}$ structure employed as a simulation input. The essential motions in S^{APO} may be linked to the structural rearrangements preventing GDP rebinding [25].

Collectively, MD simulations of the S^{GDP} and $S^{GDP'}$ forms of Sec4 display a strong tendency of SWI to detach from GDP. Such tendency is emphasized by the presence of the Sec2 GEF in the $S^{GDP'}$ trajectory.

3.1.3. Structure and dynamics of Sec4-Sec2 recognition

The analyses of flexibility and FMA suggest that the $S^{GDP'}$ form represents an evolution of the inactive G protein towards the nucleotide-depleted form.

To better characterize such form, we performed a structure network analysis of the Sec4-Sec2 interface in the MD trajectories of $S^{GDP'}$ and S^{APO}, using the crystal structure of 2OCY as a reference, which represents the Sec2-bound nucleotide-depleted state of Sec4.

In this framework, in the comparative analysis of the Sec4-Sec2 interface, we considered as rather equivalent all Sec4-Sec2 contacts involving at least one amino acid residue at a distance in the range ± 1 - ±4 residues in primary sequence from the reference residue (i.e. in the 2OCY crystal structure, Table 1, Fig. 10A).

Remarkably, the totality of identical (native) and equivalent nodes at the Sec4-Sec2 interface of $S^{GDP'}$ is 89%, indicating that, during MD simulations the input S^{GDP} $Sec4^{1G16}$ structure, pre-oriented to $Sec2^{2OCY}$, evolves towards a Sec2-bound form by conformational changes of the two switches (Fig. 10A). The simulated S^{APO} state upon removal of PO_4^{3-} from $Sec4^{2EQB}$ shares 79% of the native interface links with the 2OCY crystal structure (Fig. 10B, Table 1). This result is in line with inferences from structure determinations showing that the evolution from the PO_4^{3-}-bound 2EQB intermediate to the APO 2OCY complex involves conformational rearrangements of P-loop and other Sec4 regions, while keeping invariant the Sec4-Sec2 interface, which involves the two switch regions of the G protein [25].

Similarities in structure communication were inferred also from the metapaths computed on the $S^{GDP'}$ and S^{APO} trajectories

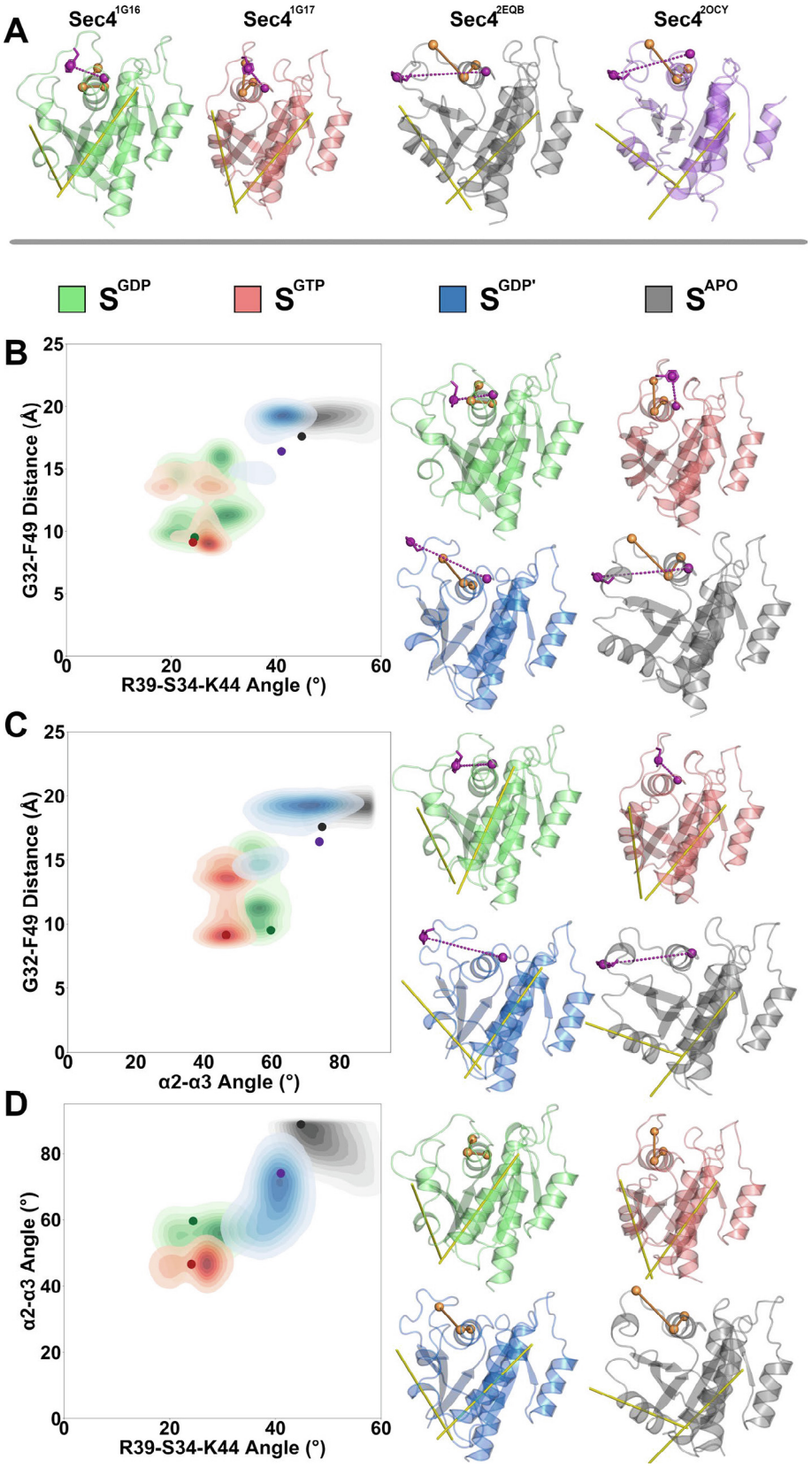

Fig. 8. Distributions of selected structural hallmarks of Sec4 states. A. The three geometrical indices: (a) the distance between the side-chain centroid of $G32^{G1:6}$ and $F49^{G2:1}$, (b) the angle among the Cα-atoms of $R39^{\alpha1:7}$, $S34^{G1:8}$, and K44, and (c) the angle between the main axes of the α2 and α3 helices are shown on the crystal structures of $Sec4^{1G16}$, $Sec4^{1G17}$, $Sec4^{2EQB}$, and $Sec4^{2OCY}$. B-D. The distribution surfaces of the conformational ensembles according to pairs of the above defined descriptors are shown for S^{GDP} (green), S^{GTP} (red), $S^{GDP'}$ (marine), and S^{APO} (grey). Dots refer to the structures used as inputs of MD simulations. For each surface plot, the representative structures of the main basins for each Sec4 simulated form are shown as cartoons with the pairs of geometrical descriptors drawn. Plots were generated by calculating the multivariate kernel density estimation of the distributions of each pair of descriptors by means of the MATLAB ver. R2018b numerical analysis package with all default parameters. (For interpretation of the references to color in this figure legend, the reader is referred to the web version of this article.)

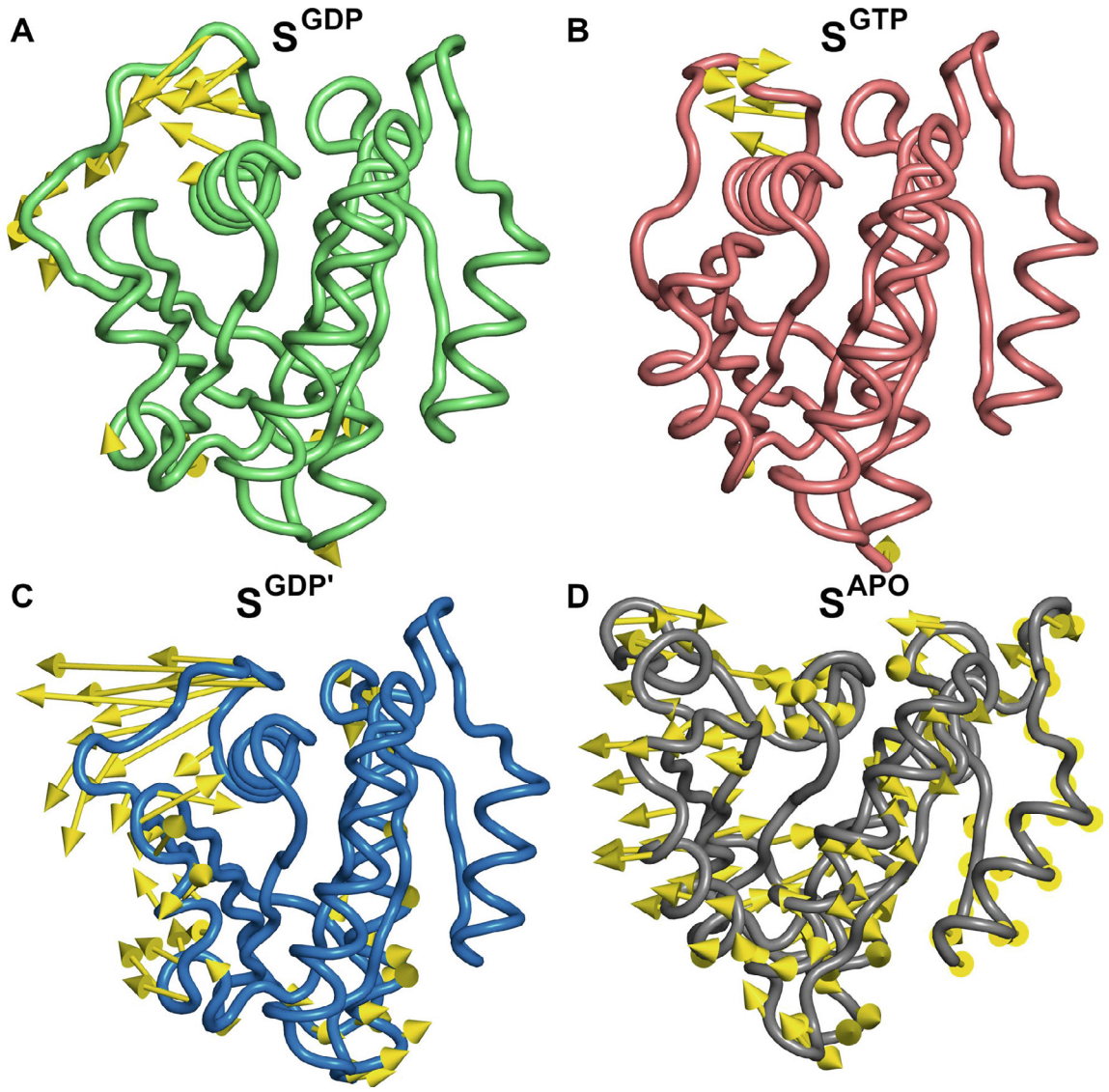

Fig. 9. Essential subspace of Sec4 functional states. The porcupine representation of the projections on the Cα-atoms of the weighted combination of the first 500 eigenvectors correlating with the angle among the Cα-atoms of $R39^{a1:7}$, $S34^{G1:8}$, and K44 is shown for (A) S^{GDP} (green), (B) S^{GTP} (red), (C) $S^{GDP'}$ (marine), and (D) S^{APO} (grey). (For interpretation of the references to color in this figure legend, the reader is referred to the web version of this article.)

(Fig. 10C,D). Indeed, both metapaths express a communication between the hydrophobic interface, which involves highly conserved amino acids (i.e. with ConSurf grades $\geq$ 7), and the *N*-terminal regions of Sec2, passing through a chain of alternate anionic and cationic amino acids with i,i + 4 or i,i + 3 patterns on $Sec2^{B}$ (i.e. E93, K89, E85, K82, and D79) (Fig. 10C,D, Supplementary Table 1 (Table S1)). This suggests that the hydrophobic interface involving SWI and SWII of Sec4 is structurally/dynamically linked to the *N*-terminal half of Sec2.

The structural coupling between Sec4-Sec2 interface and *N*-terminal regions of Sec2 reflects on the essential motions inferred from the $S^{GDP'}$ and in S^{APO} trajectories (Fig. 11). The PCA, done upon fitting all Cα-atoms in the complex, indeed shows a strong overlap between the first eigenvectors (PC1) from the two systems (overlap = 0.91). Such vectors essentially describe the bending of the *N*-terminal half of Sec2 towards Sec4. Whereas in S^{APO} Sec4 contributes poorly to PC1, in $S^{GDP'}$ all residues participate in PC1 indicative of higher mobility of Sec4 in $S^{GDP'}$ than S^{APO} because of the establishment of the inter-protein interface, upon starting from two poorly interacting proteins. Remarkably, in the S^{APO} MD trajectory started by an already formed Sec4-Sec2 interface, which does not contribute to the essential motions of the complex that instead involve the *N*-terminal half of Sec2 and the inner regions of Sec4 such as the P-loop and the C-terminal half of the G protein. This is in line with the evidences from structure determinations [25] and from the present MD simulations that the evolution from the PO_4^{3-}-bound 2EQB intermediate to the APO 2OCY complex involves deformations in the majority of Sec4 regions but those participating in the interface with Sec2 [25,26]. Some overlap also concerns PC2 of S^{APO} and PC3 of $S^{GDP'}$ (overlap = 0.78, Fig. 11).

It is worth recalling that the length of porcupines describes the maximal atomic displacement, which, however, occurs rarely in the simulation time.

Collectively, PSN and essential dynamics analysis, suggest that Sec2 assists both Sec4 deformations leading to nucleotide release and preventing GDP binding. The results also suggest that the $S^{GDP'}$ trajectory describes an evolution from the starting S^{GDP} towards S^{APO} states of Sec4.

Table 1
Links at Sec4p-Sec2p interface.

Node1[a]	Node2[a]	Pos1[b]	Cons1[c]	Cons2[c]	S^{APOd}	$S^{GDP'd}$
A88	A:N98	SWII	7	6	0	2
A88	A:V101	SWII	7	8	3	1
F45	A:K121	1α1_SWI	8	6	0	2
F45	A:Y124	1α1_SWI	8	7	0	1
F49	B:M115	SWII	5	9	0	4
F49	B:A112	SWII	5	9	2	4
F49	B:E111	SWII	5	9	2	4
F49	B:L108	SWII	5	9	0	4
F49	A:N113	SWII	5	9	2	4
F57	A:A106	SWII	8	8	0	3
F57	A:F109	SWII	8	9	0	0
F82	B:D103	SWII	8	7	0	1
F82	B:E100	SWII	8	9	0	3
F82	B:L104	SWII	8	9	0	1
I53	B:L108	SWII	8	9	2	3
I85	B:E100	SWII	7	9	0	2
K22	A:E102	β1	9	9	0	0
P47	B:M115	1α1_SWI	1	9	1	5
P47	A:N113	1α1_SWI	1	9	0	6
P47	A:V116	1α1_SWI	1	9	0	4
R81	B:D103	SWII	8	7	0	2
R81	B:S107	SWII	8	9	0	4
T52	B:E111	SWII	9	9	0	1
T84	B:E100	SWII	8	9	0	3
T84	B:K96	SWII	8	4	0	4
W74	A:F109	β3	9	9	0	6
W74	A:T105	β3	9	9	0	4
Y89	A:T105	SWII	8	9	0	1

[a]Amino acid residues from Sec4 (Node1) and Sec2 (Node 2, chains A and B) participating in stable links at the interface between Sec4 and Sec2 in the crystallographic complex encoded as 2OCY. [b]Node position in Sec4. [c]Conservation grades (according to ConSurf) of the linked nodes in Sec4 and Sec2, respectively. [d]Degree of equivalence between each 2OCY interface link and the interface link in the MD trajectories of $S^{GDP'}$ and S^{APO}. Here the numbers from 0 to 6 (i.e. n) mean that in $S^{GDP'}$ the link is contributed by identical nodes (i.e. n = 0) or by nodes found at a primary-sequence distance ± n.

3.2. Hypotheses on the early stages of Sec4 activation by Sec2

By simulating the dynamics of isolated $Sec2^{2E7S}$ and of Sec4 in four different forms the present study addressed a number of questions concerning the intrinsic and stimulated dynamics of Sec2 and Sec4 as well as the chain of structural deformations leading to GEF-assisted activation of the Rab GTPase.

First of all, MD simulations of isolated $Sec2^{2E7S}$ show that the Sec4-bound form of Sec2 (e.g. $Sec2^{2OCY}$) pre-exists to complex formation (Fig. 3), thus suggesting that Sec4 selects the Sec2 conformation suitable to productive interaction. This finding is also in line with the observation that all unbound-unbound docking simulations between $Sec4^{1G16}$ and $Sec2^{2E7S}$ followed by MD simulations failed in producing any native-like interface between the two proteins.

MD simulations of GDP-bound inactive $Sec4^{1G16}$ in a predicted complex with Sec2 ($S^{GDP'}$) highlighted early deformations in Sec4 in the path to GDP release. Indeed, a number of MD analyses, also based on structural descriptors computed on Sec4, converged into the evidence that the $S^{GDP'}$ conformational ensemble depicts an evolution of Sec4 from the S^{GDP} starting state towards the Sec2-bound S^{APO} state (Figs. 4-6, 8, and 9).

In this section, information from structure determination and from MD simulations is exploited to infer a possible temporal hierarchy of Sec2-assisted deformations in the nucleotide cage ultimately leading to GDP release.

In both $Sec4^{1G16}$ and $Sec4^{1G17}$ crystal structures the nucleotide is caged by the G-boxes and the α1/SWI loop. While G1, G2, and G3 interact with phosphates and Mg^{2+}, α1/SWI loop, G4, and G5 interact with the guanine base. As for the α1/SWI loop, F45 makes σ-π orthogonal interactions with the guanine ring, whereas the backbone carbonyl oxygen atom of P47 makes H-bonding interaction with the ribose O3′. Interactions between the P-loop and the β-phosphate and between the guanine ring and both G4 (e.g. the H-bond between the guanine and $D136^{G4:4}$) and G5 provide the most important contributions to tight binding. The crystal structure of the S29V mutant bound to GDP and Sec2 (PDB: 4ZDW), representing an intermediary state in the path to GDP release, shows still tight interaction between nucleotide and almost all G boxes, while the interactions between nucleotide and α1/SWI loop, SWI, and $D136^{G4:4}$ side-chain are lost (Figs. 12 and 13A-D).

Indeed, the distances between the centroids of the phenyl ring of F45 and of the imidazole ring of guanine (i.e. F45-guanine distance) and between the carbonyl oxygen atom of P47 and the ribose O3′-atom (i.e. P47-ribose distance) are 5.0 Å and 3.3 Å in $Sec4^{1G16}$ (starting structure of the S^{GDP} trajectory) and 4.9 Å and 3.0 Å in $Sec4^{1G17}$ (starting structure of the S^{GTP} trajectory).

In the presence of the Sec2-GEF, e.g. in the 4ZDW $Sec4^{S29V}$-GDP-Sec2 complex, those distances increase significantly, e.g. to 17.0 Å and 16.0 Å, respectively, as a consequence of the huge detachment of α1/SWI loop and SWI from GDP (Fig. 12).

We recall that formation of the S^{GTP} state is also associated with formation of two sites of interactions (Site 1 and Site 2) between the two switches, which are absent in S^{GDP} (Fig. 2).

To infer a tentative temporal hierarchy in nucleotide-cage deformations, we chose the combination of F45-guanine distance and the plane-angle among the Cα-atoms of $R39^{α1:7}$, $S34^{G1:8}$, and K44, accounting for the deformations of P-loop (G1) and SWI (G2), as descriptors of the nucleotide exchange process (Fig. 12). In this context, the P47-ribose distance works similarly to the F45-guanine distance. Both distance and angle increase in the presence of Sec2 and separate the Sec2-bound from the Sec2-free states of Sec4 (Fig. 12A). Remarkably, in S^{GDP}, the interaction between F45 and the nucleotide tend to be lost even in the absence of Sec2 (Fig. 12A,B and Fig. 13A). Indeed, in the representative structure of one of the two almost equi-populated basins, the F45-guanine distance is 7.7 Å (Fig. 12A), which is higher than the value in the starting crystal structure ($Sec4^{1G16}$, 5.0 Å). In the representative

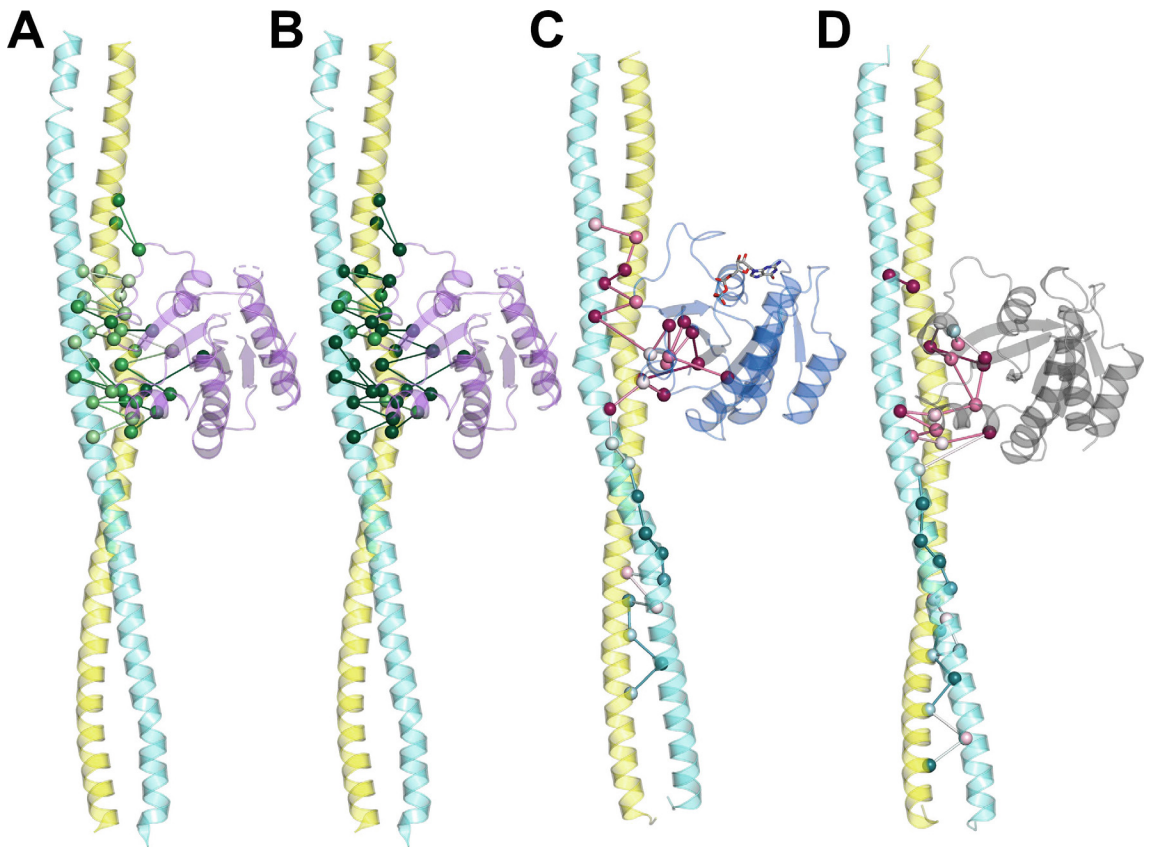

Fig. 10. Structural communication in Sec4-Sec2 complexes. Comparisons of the interface-links between $S^{GDP'}$ (A) and S^{APO} (B) are shown mapped on the S^{2OCY} crystal structure. Link color goes from dark green to white through five intermediate shades depending on decreasing equivalence between $S^{GDP'}$ or S^{APO} and the S^{2OCY} crystal structure. In detail, the dark green means identity whereas the green shades to white mean that in $S^{GDP'}$ or S^{APO} the link is contributed by nodes found at a primary-sequence distance ± n (where n goes from 1 to 6 (white)) from those contributing to the interface link in to S^{2OCY} crystal structure. Each node is colored according to the average degree of equivalence of its links. C,D. Metapaths are shown mapped on the structures of $S^{GDP'}$ (C) and S^{APO} (D) closest to the average. Metapaths are colored according to the conservation grades inferred from the ConSurf web server (https://consurf.tau.ac.il). (For interpretation of the references to color in this figure legend, the reader is referred to the web version of this article.)

structure of the main basin concerning the $S^{GDP'}$ trajectory, the F45-guanine distance increases to 13.6 Å, reaching a maximum of 25.5 Å within the conformational ensemble (Fig. 12B).

All together, these results show that early deformations in the nucleotide cage concern the α1/SWI loop and SWI. In the structure from MD simulations of $S^{GDP'}$ closest to the crystallographic Sec4-Sec2 complex (Fig. 13B), the α1/SWI loop approaches $Sec2^{A}$ driven by the establishment of a persistent $D43^{Sec4}$-$K121^{Sec2}$ interaction (Fig. 13B). The residues K44 and F45, in such loop, approach $Y124^{Sec2A}$. Another remarkable feature of $S^{GDP'}$, which is shared with all crystallographic Sec4-Sec2 complexes, is formation of specific interactions between the two switches characterizing Site 1 ($I55^{SWI:7}$-$W74^{β3:6}$-$Y89^{SWII:15}$, Figs. 2 and 13B-D). Site 1 and α2, which is part of SWII, participate in the interface with Sec2.

Remarkably, while establishing contacts with Sec2, α2 becomes almost orthogonal to α3. This is another deformation of Sec4 shared by the Sec2-bound forms, which emerges already from the $S^{GDP'}$ conformational ensemble (Fig. 13B). However, due to the less structured state of α2 in $S^{GDP'}$ compared to the Sec4-Sec2 crystallographic complexes, the side chain of $Y89^{SWII:10}$ is still directed towards the parallel β-sheet of Sec4 instead of turning and participating in the hydrophobic interface with Sec2 (Figs. 2 and 13B-D).

Collectively, the amino acids forming a hydrophobic cluster at the Sec4-Sec2 interface are the same in $S^{GDP'}$ and the crystallographic Sec2-Sec4 complexes. However, due to the incomplete conformational transitions of the two switch regions in $S^{GDP'}$ compared to the Sec4-Sec2 crystallographic complexes, the stereochemistry of the interface and the details of the inter-residue interactions are different (Table 1 and Fig. 13B-D). In $S^{GDP'}$, the nucleotide completely looses all interactions with α1/SWI loop and SWI while retaining all other interactions characterizing the S^{GDP} state. (Fig. 13A,B).

By integrating the information from structure determination and molecular simulations the following mechanistic picture can be drown: 1) Sec4 selects a Sec2 conformation suitable to form the proper interface with Sec2 (Fig. 13); 2) the establishment of the $K22^{β1:3}$-$E102^{Sec2A}$ salt bridge and hydrophobic interactions between the C-terminal end of SWI and $F109^{Sec2A}$, $L104^{Sec2B}$, and $L108^{Sec2B}$ contributes to early anchoring of Sec4 to Sec2 (Fig. 13A); 3) the α1/SWI loop and SWI, pulled by Sec2 on itself, loose their contacts with GDP (Fig. 13B-D); 4) Site 1 interactions between SWI and SWII form (Fig. 13B-D); 5) the main axis of α2 (belonging to SWII) becomes orthogonal to α3 (Fig. 13B-D); 6) SWII folds in a 3-turn α-helix allowing for completion of the Sec4-Sec2 interface that is largely hydrophobic (Fig. 13C); 7) the H-bonding interactions between guanine ring and $D136^{G4:4}$ breaks possibly destabilizing also the interactions with both G4 and G5 (Fig. 13C); and 8) final conformational changes of P-loop, SWI and SWII (i.e. G1, G2, and G3) occur leading to GDP release (Fig. 13D).

The spontaneous acquisition of a Sec4-bound state by Sec2 and all Sec2-assisted deformations of Sec4 listed at points 3–6 above are likely to occur on fast time-scales as they could be observed

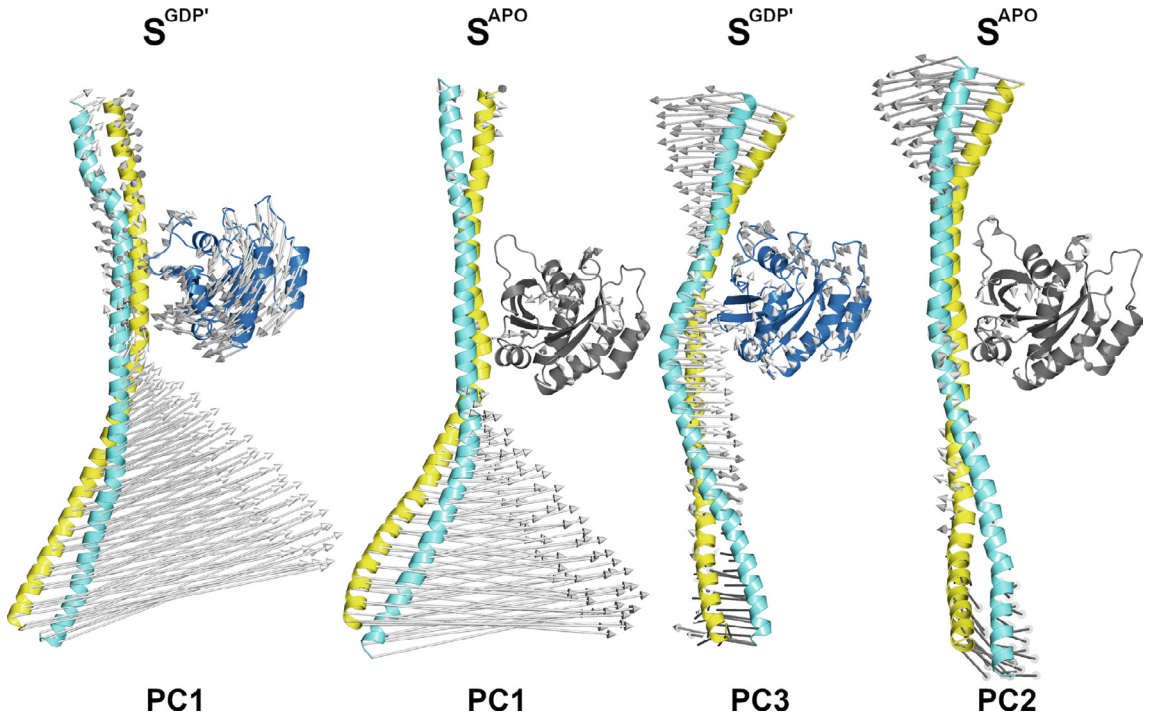

Fig. 11. Essential motions of the Sec4-Sec2 complexes. The porcupine representations of PC1 and PC3 concerning $S^{GDP'}$ and those of PC1 and PC2 concerning S^{APO} are shown. The two PC1 have a 0.91 overlap, whereas PC3 and PC2 have a 0.78 overlap.

in microsecond MD simulations. In contrast, Sec2-assisted deformations of Sec4 listed at points 7–9 above are likely to require longer time-scales.

4. Discussion

We have been investigating since long functional dynamics and structural communication in Ras GTPases [14,56–60]. PCA and Elastic Network Model-Normal Mode Analysis (ENM-NMA) were exploited to identify the important structural flexibilities that enable proteins in the Ras superfamily to switch between their active and inactive states [21]. The study led to a hypothesis on the evolutionary adaptation of structural deformations by the individual members of the superfamily to fulfill their specialized function. The deformation modes, which allow the Ras GTPases to accomplish their switching function, are conserved along evolution and reside in the *N*-terminal lobe-1 portions comprising the two switches [21]. These modes lead to functional specialization when associated with evolution-driven deformations of protein portions essentially located in lobe 2, distal from the nucleotide. Consistently, high pressure crystallography indicated that the complex interplay between *N*-terminal and C-terminal lobes (i.e. effector and allosteric lobes, respectively) is directly linked to Ras cycling [63].

A combination of ENM-NMA with PSN analysis, in a so-called mixed PSN-ENM approach to infer structural communication pathways from single crystallographic structures, served to dissect functional dynamics and structural communication in GEFs specialized for Rho GTPases (RhoGEFs), which hold the DH and PH domains [64]. The study inferred major evolutionary-driven deformations related to the mechanisms adopted by the GEF to prevent Rho binding (i.e. functional specialization linked to auto-inhibition). MD simulations on isolated and RhoGEF-bound RhoA strengthened the scaffolding action of the DH domain, which primarily turns the SWI of RhoA on itself and enhances the flexibility of the nucleotide binding regions, weakening the connections between GDP and G-boxes [61].

In line with computational investigation of RhoGEF action, the present study employed microsecond MD simulation and established analysis tools to infer hypotheses on the mechanism of GDP release from another Ras GTPase, Sec4, belonging to the Rab family. In general, whereas Ras GTPases are structurally very conserved, GEFs are specific for each family and completely structurally unrelated. Exemplar of this is the fact that RhoGEFs belong to the Dbl family and hold the DH and PH domains, whereas Sec2 is made of a coiled-coil helix dimer. Yet, the RhoA and Rab regions deputed to GEF binding and nucleotide release are the same (i.e. the two switch regions and the inter-switch).

Remarkably, we found that Sec2 has an intrinsic ability to adopt the conformation found in the crystallographic complexes with Sec4, thus suggesting that the latter selects and shifts the conformational equilibrium of the GEF towards a pre-existing bound-like conformation rather than inducing it. In contrast, simulations of Sec4 in the S^{GDP} state could not find any Sec2-bound conformation, which may be linked, at least in part, to the more complex energy landscape of the Rab protein compared to the cognate GEF. Deformations of the GDP-bound form towards the APO form of Sec4 could be partially observed only in the presence of Sec2. Indeed, MD simulations of early deformations in the transition from S^{GDP} to S^{APO} led to the $S^{GDP'}$ conformational ensemble, characterized by pulling of SWI on Sec2 and consequent displacement of the α1/SWI loop and the whole SWI away from the nucleotide cage. Formation of Sec2-Sec4 interface was accompanied by extensions of both β2 and β3 strands and formation of Site1-interactions between the two switches in preparation of the active state. Preliminary folding and re-orientation towards Sec2 of SWII was also observed. Although productive deformations leading to GDP release require the presence of Sec2, some of those deformations could be already observed in the conformational ensemble characterizing

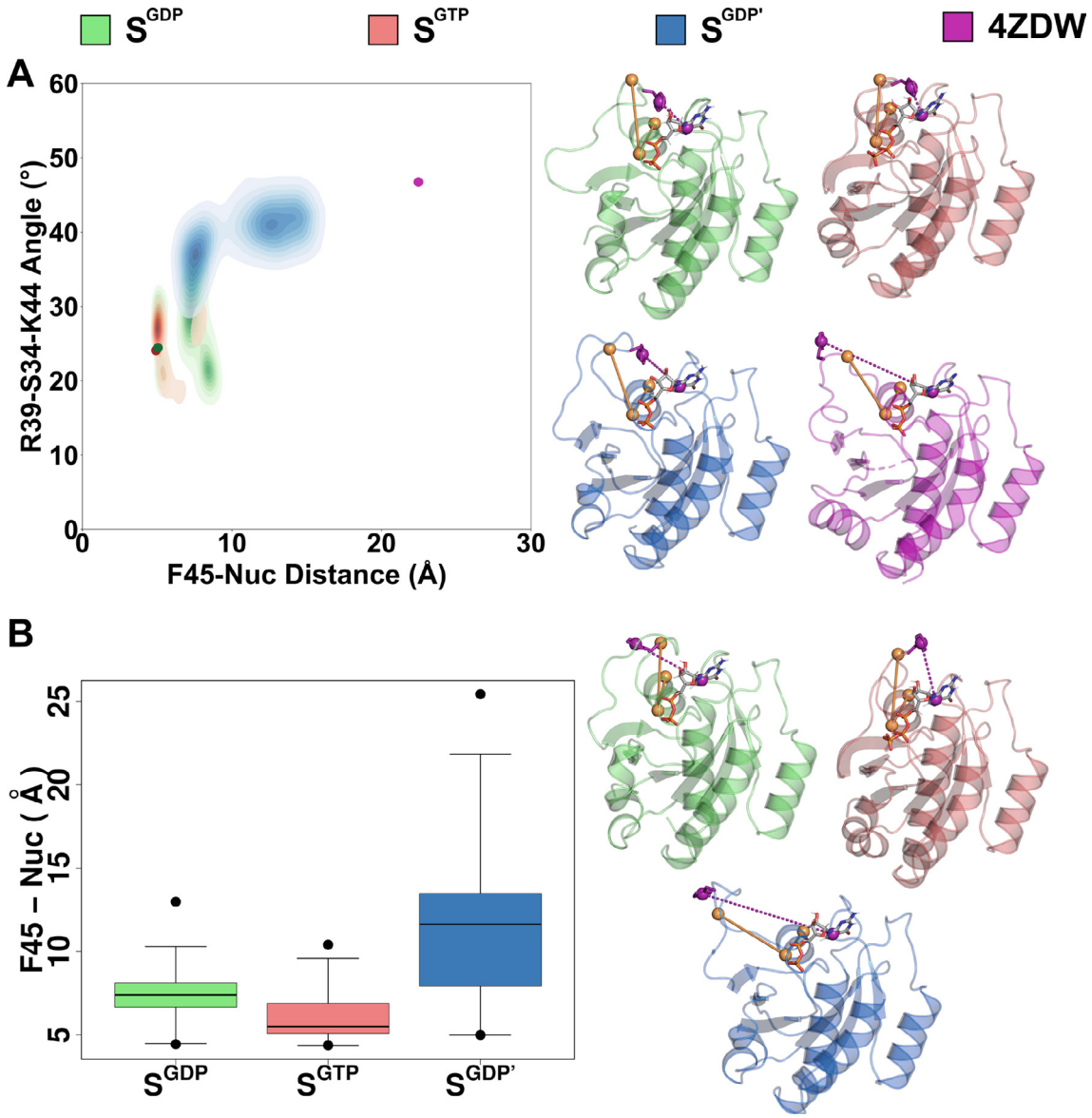

Fig. 12. Distributions of structural hallmarks of nucleotide-cage deformation. A. The geometrical indices: R39$^{\alpha1:7}$, S34$^{G1:8}$, and K44, and the distance between F45 centroid and guanine pentatomic-ring centroid (i.e. F45-Nuc distance) are used as coordinates in population surface plots concerning the Sec4 forms S^{GDP} (green), S^{GTP} (red), and $S^{GDP'}$ (marine). Dots refer to the structures used as inputs of MD simulations. The magenta dot refers to the crystal structure of GDP-bound S29V mutant of Sec4 in complex with Sec2 (PDB: 4ZDW). On the right side, the representative structures of the main basins for each simulated form of Sec4 are shown as cartoons with the pairs of geometrical descriptors drawn. Cartoons of the 4ZDW crystal structure together with the geometrical descriptors are shown as well. B. Box-plots of the F45-Nuc distance are shown. On the right side, the structures corresponding to the frames with the maximal F45-Nuc distance are shown as cartoons with the pairs of geometrical descriptors drawn. Surface plots were generated by calculating the multivariate kernel density estimation of the distributions of each pair of descriptors by means of the MATLAB ver. R2018b numerical analysis package with all default parameters. (For interpretation of the references to color in this figure legend, the reader is referred to the web version of this article.)

the inactive S^{GDP} state. Some of them include loss of the F45-guanine interaction that characterizes the crystal structures of isolated Sec4 and formation of Site 1 interactions observed in all crystallographic complexes between Sec4 and Sec2, thus highlighting an intrinsic ability of the Rab protein to loose interactions between nucleotide and α1/SWI loop and SWI. All together these features may be linked, at least in part, to the rather high rate of nucleotide dissociation by Sec4.

Whereas pulling of α1/SWI loop and SWI on Sec2 and formation of Site 1 occur early in the process of GDP release, the establishment of the native hydrophobic Sec2-Sec4 interface participated by SWI and SWII is slower as it requires a re-organization of the interface between SWII and both β1 and β3, accompanied by extension and re-orientation of α2 (which is part of SWII). Thus, the rearrangement of the hydrophobic interface leading to the final deformations of the G boxes, in particular G1-3, could not be observed in $S^{GDP'}$ trajectory. In the Sec4-Sec2 system, such event is likely linked to the establishment of a structural communication between the hydrophobic interface and the *N*-terminal portion of the GEF. In this respect, differently from the RhoGEF DH, which essentially acts as a scaffold for RhoA binding, Sec2 seems to dynamically aid Sec4 transformation.

In summary, the results of computational experiments, integrated with structure determinations, suggest that Sec4 selects the suitable conformation of Sec2, by establishing early

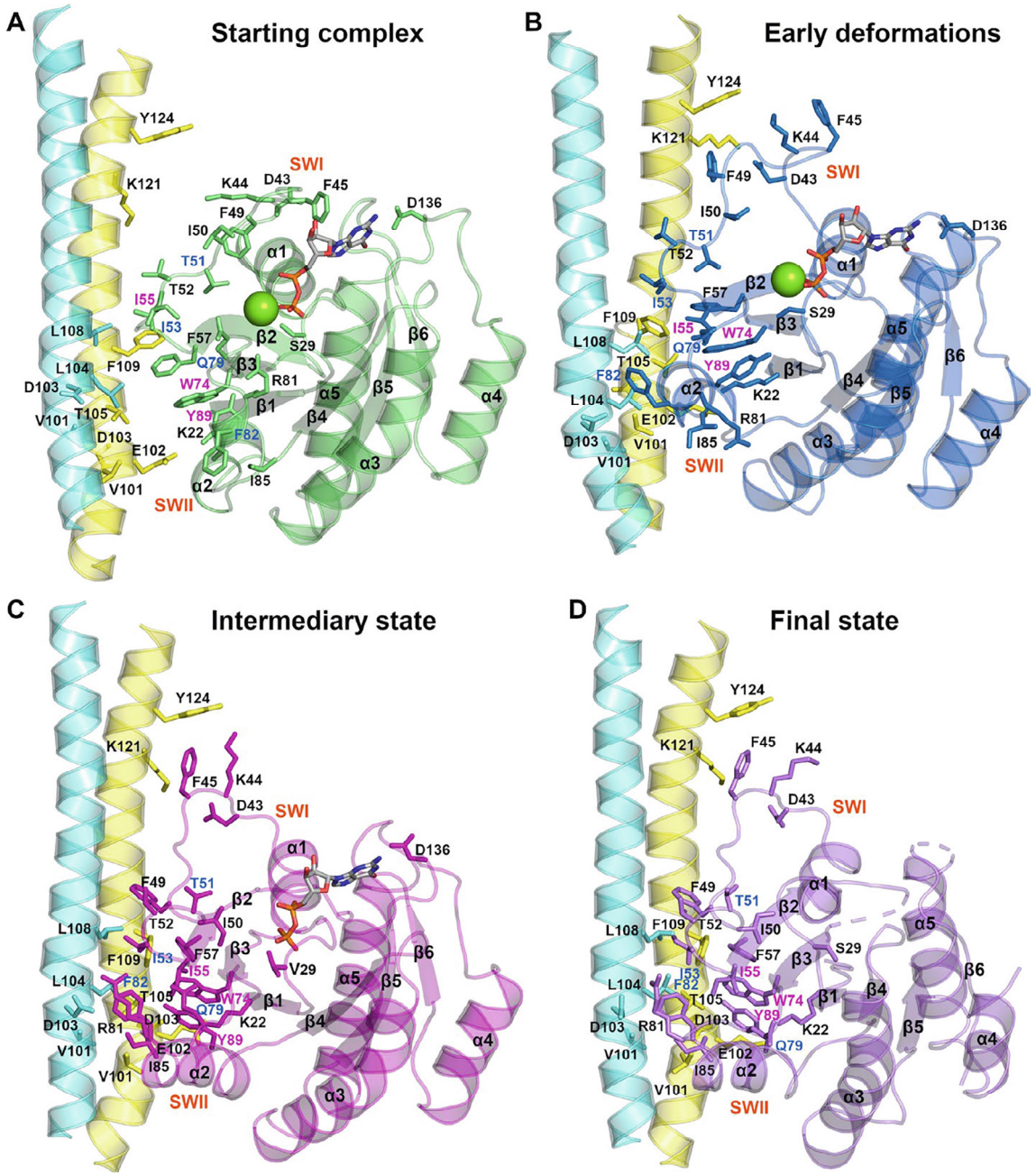

Fig. 13. Sec4 deformations leading to GDP release. A. The complex between Sec2 from the 2OCY crystal structure and the crystal structure of S^{GDP} Sec4 (PDB: 1G16) used as an input of MD simulation of the $S^{GDP'}$ form is shown. B. The structure most similar to the 2EQB crystallographic complex from the $S^{GDP'}$ trajectory is shown. The crystal structures of Sec2 in complex with the GDP-bound S29V mutant of Sec4 (PDB: 4ZDW, C) and APO Sec4 (PDB: 2OCY, D) are shown. The labels of those amino acid residues, which in S^{GTP} participate in Site 1 and Site 2, are magenta and blue, respectively. The two coiled-coil helices of Sec2 are yellow (chain A) and aquamarine (chain B), whereas $Sec4^{1G16}$, Sec4 $S^{GDP'}$, $Sec4^{4ZDW}$, and $Sec4^{2OCY}$ are, respectively, green, marine, magenta, and violet. The side chains participating in Sites 1 and 2 or in the interface between Sec4 and Sec2 are shown in sticks. The nucleotide is shown in sticks as well, colored by atom type. The Mg^{2+} ion in $Sec4^{1G16}$ and Sec4 $S^{GDP'}$ is represented as green sphere. The secondary structure elements are labeled according to the Noel's nomenclature [20]. (For interpretation of the references to color in this figure legend, the reader is referred to the web version of this article.)

interactions such as the $K22^{\beta1:3}$-$E102^{Sec2A}$ salt bridge and a provisional hydrophobic interface. This favors Sec2-assisted pulling on itself of the α1/SWI loop and SWI, which loose any contact with GDP. Pulling of α1/SWI loop and SWI, formation of SWI-SWII Site 1 interaction, and rotation of α2 likely occur earlier. Formation of the final hydrophobic interface, which would require final deformations of SWI and SWII, accomplishes later. Disruption of the nucleotide cage would cause firstly the loss of interactions with the guanine ring and secondly the loss of interactions with the phosphates.

In line with the results of high pressure crystallography determinations on Ras, revealing the multiplicity of sub-states with many transient intermediates [63], the dynamics of Sec4 is more complex than that of its GEF, which may relate to the latter acting

as a catalyst. Indeed, the ease in sampling the energy landscape and adopting a bound-like conformation likely favors the catalyzing ability of a Ras GTPase GEF.

Funding

This study was supported by Airc-Italy [IG14811] and PRIN2017 MIUR grants to FF.

Declaration of Competing Interest

The authors declare that they have no known competing financial interests or personal relationships that could have appeared to influence the work reported in this paper.

Appendix A. Supplementary data

Supplementary data to this article can be found online at https://doi.org/10.1016/j.csbj.2022.09.016.

References

[1] Vetter IR, Wittinghofer A. The guanine nucleotide-binding switch in three dimensions. Science 2001;294(5545):1299–304.
[2] Colicelli J. Human RAS superfamily proteins and related GTPases. Sci STKE 2004;2004(250):RE13.
[3] Wittinghofer A, Vetter IR. Structure-function relationships of the G domain, a canonical switch motif. Annu Rev Biochem 2011;80:943–71.
[4] Grosshans BL, Ortiz D, Novick P. Rabs and their effectors: achieving specificity in membrane traffic. Proc Natl Acad Sci U S A 2006;103(32):11821–7.
[5] Bos JL, Rehmann H, Wittinghofer A. GEFs and GAPs: Critical elements in the control of small G proteins (vol 129, pg 865, 2007). Cell 2007;130(2):385.
[6] Aittaleb M, Gao G, Evelyn CR, Neubig RR, Tesmer JJ. A conserved hydrophobic surface of the LARG pleckstrin homology domain is critical for RhoA activation in cells. Cell Signal 2009;21(11):1569–78.
[7] Rossman KL, Der CJ, Sondek J. GEF means go: Turning on Rho GTPases with guanine nucleotide-exchange factors. Nat Rev Mol Cell Biol 2005;6(2):167–80.
[8] Snyder JT, Worthylake DK, Rossman KL, Betts L, Pruitt WM, Siderovski DP, et al. Structural basis for the selective activation of Rho GTPases by Dbl exchange factors. Nat Struct Biol 2002;9(6):468–75.
[9] Mori K, Hata M, Neya S, Hoshino T. Common semiopen conformations of Mg2+-free Ras, Rho, Rab, Arf, and Ran proteins combined with GDP and their similarity with GEF-bound forms. J Am Chem Soc 2005;127(43):15127–37.
[10] Xiong Y, Zeng J, Xia F, Cui Q, Deng X, Xu X. Conformations and binding pockets of HRas and its guanine nucleotide exchange factors complexes in the guanosine triphosphate exchange process. J Comput Chem 2022;43(13):906–16.
[11] Rasmussen SG, Devree BT, Zou Y, Kruse AC, Chung KY, Kobilka TS, et al. Crystal structure of the beta(2) adrenergic receptor-Gs protein complex. Nature 2011;469:175–81.
[12] Kang YY, Kuybeda O, de Waal PW, Mukherjee S, Van Eps N, Dutka P, et al. Cryo-EM structure of human rhodopsin bound to an inhibitory G protein. Nature 2018;558(7711). 553-+.
[13] Dror RO, Mildorf TJ, Hilger D, Manglik A, Borhani DW, Arlow DH, et al. SIGNAL TRANSDUCTION. Structural basis for nucleotide exchange in heterotrimeric G proteins. Science 2015;348(6241):1361–5.
[14] Raimondi F, Seeber M, Benedetti PG, Fanelli F. Mechanisms of inter- and intramolecular communication in GPCRs and G proteins. J Am Chem Soc 2008;130(13):4310–25.
[15] Gorfe AA, Grant BJ, McCammon JA. Mapping the nucleotide and isoform-dependent structural and dynamical features of ras proteins. Structure 2008;16(6):885–96.
[16] Grant BJ, Gorfe AA, McCammon JA. Ras Conformational Switching: Simulating Nucleotide-Dependent Conformational Transitions with Accelerated Molecular Dynamics. PLoS Comput Biol 2009;5(3):e1000325.
[17] Kosztin I, Bruinsma R, O'Lague P, Schulten K. Mechanical force generation by G proteins. Proc Natl Acad Sci U S A 2002;99(6):3575–80.
[18] Ma JP, Karplus M. Ligand-induced conformational changes in ras p21: A normal mode and energy minimization analysis. J Mol Biol 1997;274(1):114–31.
[19] Ma JP, Karplus M. Molecular switch in signal transduction: Reaction paths of the conformational changes in ras p21. PNAS 1997;94(22):11905–10.
[20] Noel JP, Hamm HE, Sigler PB. The 2.2 A crystal structure of transducin-alpha complexed with GTP gamma S. Nature 1993;366(6456):654–63.
[21] Raimondi F, Orozco M, Fanelli F. Deciphering the deformation modes associated with function retention and specialization in members of the Ras superfamily. Structure 2010;18(3):402–14.
[22] Stroupe C, Brunger AT. Crystal structures of a Rab protein in its inactive and active conformations. J Mol Biol 2000;304(4):585–98.
[23] Itzen A, Rak A, Goody RS. Sec2 is a highly efficient exchange factor for the Rab protein Sec4. J Mol Biol 2007;365(5):1359–67.
[24] Sato Y, Shirakawa R, Horiuchi H, Dohmae N, Fukai S, Nureki O. Asymmetric coiled-coil structure with Guanine nucleotide exchange activity. Structure 2007;15(2):245–52.
[25] Sato Y, Fukai S, Ishitani R, Nureki O. Crystal structure of the Sec4p.Sec2p complex in the nucleotide exchanging intermediate state. Proc Natl Acad Sci U S A 2007;104(20):8305–10.
[26] Dong G, Medkova M, Novick P, Reinisch KM. A catalytic coiled coil: structural insights into the activation of the Rab GTPase Sec4p by Sec2p. Mol Cell 2007;25(3):455–62.
[27] Rinaldi FC, Packer M, Collins R. New insights into the molecular mechanism of the Rab GTPase Sec4p activation. BMC Struct Biol 2015;15:14.
[28] Hess B, Kutzner C, Van Der Spoel D, Lindahl E. GROMACS 4: Algorithms for Highly Efficient, Load-Balanced, and Scalable Molecular Simulation. J Chem Theory Comput 2008;4:435–47.
[29] Leaver-Fay A, Tyka M, Lewis SM, Lange OF, Thompson J, Jacak R, et al. ROSETTA3: an object-oriented software suite for the simulation and design of macromolecules. Methods Enzymol 2011;487:545–74.
[30] Gray JJ, Moughon S, Wang C, Schueler-Furman O, Kuhlman B, Rohl CA, et al. Protein-protein docking with simultaneous optimization of rigid-body displacement and side-chain conformations. J Mol Biol 2003;331(1):281–99.
[31] Chaudhury S, Berrondo M, Weitzner BD, Muthu P, Bergman H, Gray JJ. Benchmarking and Analysis of Protein Docking Performance in Rosetta v3.2. PLoS ONE 2011;6(8).
[32] Wang C, Schueler-Furman O, Baker D. Improved side-chain modeling for protein-protein docking. Protein Sci 2005;14(5):1328–39.
[33] Wang C, Bradley P, Baker D. Protein-protein docking with backbone flexibility. J Mol Biol 2007;373(2):503–19.
[34] Seeber M, Felline A, Raimondi F, Muff S, Friedman R, Rao F, et al. Wordom: A user-friendly program for the analysis of molecular structures, trajectories, and free energy surfaces. J Comput Chem 2011;32(6):1183–94.
[35] Sorin EJ, Pande VS. Exploring the helix-coil transition via all-atom equilibrium ensemble simulations. Biophys J 2005;88(4):2472–93.
[36] Meagher KL, Redman LT, Carlson HA. Development of polyphosphate parameters for use with the AMBER force field. J Comput Chem 2003;24(9):1016–25.
[37] Bussi G, Donadio D, Parrinello M. Canonical sampling through velocity rescaling. J Chem Phys 2007;126(1):014101.
[38] Berendsen HJC, Postma JPM, Vangunsteren WF, Dinola A, Haak JR. Molecular-Dynamics with Coupling to an External Bath. J Chem Phys 1984;81(8):3684–90.
[39] Hess B, Bekker H, Berendsen HJC, Fraaije JGEM. LINCS: A linear constraint solver for molecular simulations. J Comput Chem 1997;18(12):1463–72.
[40] Felline A, Seeber M, Fanelli F. PSNtools for standalone and web-based structure network analyses of conformational ensembles. Comput Struct Biotechnol J 2022;20:640–9.
[41] Navizet I, Cailliez F, Lavery R. Probing protein mechanics: Residue-level properties and their use in defining domains. Biophys J 2004;87(3):1426–35.
[42] Lavery R, Sacquin-Mora S. Protein mechanics: a route from structure to function. J Biosci 2007;32(5):891–8.
[43] Sacquin-Mora S, Laforet E, Lavery R. Locating the active sites of enzymes using mechanical properties. Proteins-Struct Funct Bioinf 2007;67(2):350–9.
[44] Munz M, Hein J, Biggin PC. The role of flexibility and conformational selection in the binding promiscuity of PDZ domains. PLoS Comput Biol 2012;8(11):e1002749.
[45] Amadei A, Linssen AB, Berendsen HJ. Essential dynamics of proteins. Proteins 1993;17(4):412–25.
[46] Hub JS, de Groot BL. Detection of functional modes in protein dynamics. PLoS Comput Biol 2009;5(8):e1000480.
[47] Vishveshwara S, Brinda KV, Kannan N. Protein structure: insights from graph theory. J Theor Comput Chem 2002;1:187–211.
[48] Felline A, Seeber M, Fanelli F. webPSN v2.0: a webserver to infer fingerprints of structural communication in biomacromolecules. Nucleic Acids Res 2020;48(W1):W94–W103.
[49] Raimondi F, Felline A, Seeber M, Mariani S, Fanelli F. A Mixed Protein Structure Network and Elastic Network Model Approach to Predict the Structural Communication in Biomolecular Systems: The PDZ2 Domain from Tyrosine Phosphatase 1E As a Case Study. J Chem Theory Comput 2013;9:2504–18.
[50] Vishveshwara S, Ghosh A, Hansia P. Intra and inter-molecular communications through protein structure network. Curr Protein Pept Sci 2009;10(2):146–60.
[51] Brinda KV, Vishveshwara S. A network representation of protein structures: implications for protein stability. Biophys J 2005;89(6):4159–70.
[52] del Sol A, Fujihashi H, Amoros D, Nussinov R. Residues crucial for maintaining short paths in network communication mediate signaling in proteins. Mol Syst Biol 2006;2006(2):0019.
[53] del Sol A, Fujihashi H, Amoros D, Nussinov R. Residue centrality, functionally important residues, and active site shape: analysis of enzyme and non-enzyme families. Protein Sci 2006;15(9):2120–8.
[54] Dijkstra EW. A Note on Two Problems in Connexion with Graphs. Numer Math 1959;1:269–71.
[55] Ashkenazy H, Abadi S, Martz E, Chay O, Mayrose I, Pupko T, et al. ConSurf 2016: an improved methodology to estimate and visualize evolutionary conservation in macromolecules. Nucleic Acids Res 2016;44(W1):W344–50.

[56] Felline A, Mariani S, Raimondi F, Bellucci L, Fanelli F. Structural Determinants of Constitutive Activation of Gα Proteins: Transducin as a Paradigm. J Chem Theory Comput 2017;13:886–99.
[57] Mariani S, Dell'Orco D, Felline A, Raimondi F, Fanelli F. Network and atomistic simulations unveil the structural determinants of mutations linked to retinal diseases. PLoS Comput Biol 2013;9(8):e1003207.
[58] Raimondi F, Felline A, Portella G, Orozco M, Fanelli F. Light on the structural communication in Ras GTPases. J Biomol Struct Dyn 2013;31(2):142–57.
[59] Raimondi F, Portella G, Orozco M, Fanelli F. Nucleotide binding switches the information flow in ras GTPases. PLoS Comput Biol 2011;7(3):e1001098.
[60] Fanelli F, De Benedetti PG. Update 1 of: Computational Modeling Approaches to Structure-Function Analysis of G Protein-Coupled Receptors. Chem Rev 2011;111(12):PR438–535.
[61] Felline A, Belmonte L, Raimondi F, Bellucci L, Fanelli F. Interconnecting Flexibility, Structural Communication, and Function in RhoGEF Oncoproteins. J Chem Inf Model 2019;59(10):4300–13.
[62] Sacquin-Mora S. Fold and flexibility: what can proteins' mechanical properties tell us about their folding nucleus? J R Soc Interface 2015;12(112).
[63] Girard E, Lopes P, Spoerner M, Dhaussy AC, Prange T, Kalbitzer HR, et al. Equilibria between conformational states of the Ras oncogene protein revealed by high pressure crystallography. Chem Sci 2022;13(7):2001–10.
[64] Raimondi F, Felline A, Fanelli F. Catching Functional Modes and Structural Communication in Dbl Family Rho Guanine Nucleotide Exchange Factors. J Chem Inf Model 2015;55:1878–93.